AGU PUBLICATIONS

Paleoceanography

RESEARCH ARTICLE
10.1002/2014PA002670

Key Points:
- Uniform surface to bottom temperature increase during MECO
- No water column stratification or primary productivity changes during MECO
- Warming may have directly affected pelagic and benthic ecosystems

Supporting Information:
- Readme
- Table S1
- Figure S1
- Figure S2

Correspondence to:
F. Boscolo Galazzo,
flavia.boscologalazzo@studenti.unipd.it;
flavia.boscologalazzo@unipd.it

Citation:
Boscolo Galazzo, F., E. Thomas, M. Pagani, C. Warren, V. Luciani, and L. Giusberti (2014), The middle Eocene climatic optimum (MECO): A multiproxy record of paleoceanographic changes in the southeast Atlantic (ODP Site 1263, Walvis Ridge), *Paleoceanography*, *29*, 1143–1161, doi:10.1002/2014PA002670.

Received 9 MAY 2014
Accepted 3 NOV 2014
Accepted article online 6 NOV 2014
Published online 8 DEC 2014

The middle Eocene climatic optimum (MECO): A multiproxy record of paleoceanographic changes in the southeast Atlantic (ODP Site 1263, Walvis Ridge)

F. Boscolo Galazzo[1], E. Thomas[2,3], M. Pagani[2], C. Warren[2], V. Luciani[4], and L. Giusberti[1]

[1]Department of Geosciences, University of Padova, Padova, Italy, [2]Department of Geology and Geophysics, Yale University, New Haven, Connecticut, USA, [3]Department of Earth and Environmental Sciences, Wesleyan University, Middletown, Connecticut, USA, [4]Department of Physics and Earth Sciences, University of Ferrara, Ferrara, Italy

Abstract The middle Eocene climatic optimum (MECO, ~40 Ma) was a transient period of global warming that interrupted the secular Cenozoic cooling trend. We investigated the paleoceanographic, paleoenvironmental, and paleoecological repercussions of the MECO in the southeast Atlantic subtropical gyre (Ocean Drilling Program Site 1263). TEX_{86} and $\delta^{18}O$ records support an ~4°C increase in surface and deepwater temperatures during the MECO. There is no long-term negative carbon isotope excursion (CIE) associated with the early warming, consistent with other sites, and there is no short-term negative CIE (~50 kyr) during the peak of the MECO, in contrast to what has been observed at some sites. This lack of a CIE during the peak of the MECO at Site 1263 could be due to poor sediment recovery or geographic heterogeneity of the $\delta^{13}C$ signal. Benthic and planktic foraminiferal mass accumulation rates markedly declined during MECO, indicating a reduction of planktic foraminiferal production and export productivity. Vertical $\delta^{13}C$ gradients do not indicate major changes in water column stratification, and there is no biomarker or micropaleontological evidence that hypoxia developed. We suggest that temperature dependency of metabolic rates could explain the observed decrease in foraminiferal productivity during warming. The kinetics of biochemical reactions increase with temperature, more so for heterotrophs than for autotrophs. Steady warming during MECO may have enhanced heterotroph (i.e., foraminiferal) metabolic rates, so that they required more nutrients. These additional nutrients were not available because of the oligotrophic conditions in the region and the lesser response of primary producers to warming. The combination of warming and heterotroph starvation altered pelagic food webs, increased water column recycling of organic carbon, and decreased the amount of organic carbon available to the benthos.

1. Introduction

The middle Eocene climatic optimum (MECO) is a global warming event which temporarily interrupted the long-term cooling trend initiated at the end of the early Eocene climate optimum (EECO, ~49 Ma). The MECO was first recognized by an ~1‰ negative oxygen isotope excursion in bulk carbonate and benthic foraminiferal tests in Southern Ocean cores [*Bohaty and Zachos*, 2003], and subsequently identified in the Atlantic Ocean, and central western Tethys [*Jovane et al*., 2007; *Bohaty et al*., 2009; *Edgar et al*., 2010; *Spofforth et al*., 2010]. Bulk carbonate oxygen isotope records indicate ~4–6°C warming (assuming ice-free conditions), with a gradual onset and brief peak temperatures, followed by a rapid return to preevent temperatures. The available benthic foraminiferal oxygen isotope records, mostly from the Southern Ocean, are similar. High-resolution stratigraphic analysis of cores from Site 1260 (tropical west Atlantic) indicates that the warming event lasted between 400 and 500 kyr, with a gradual onset starting at ~40.45–40.5 Ma and peak warming by 40.05 + 0.02 Ma [*Bohaty et al*., 2009; *Westerhold and Röhl*, 2013]. The MECO occurred during a very long eccentricity cycle minimum, thus at relatively attenuated seasonality at lower latitudes [*Westerhold and Röhl*, 2013]. Its duration and pattern of warming differentiate the MECO from upper Paleocene-lower Eocene hyperthermal events [*Bohaty et al*., 2009], which are characterized by more symmetrical patterns of warming and cooling that lasted a few tens of thousands of years and generally occurred during eccentricity maxima [*Thomas and Zachos*, 2000; *Cramer et al*., 2003; *Bowen and Zachos*, 2010; *Galeotti et al*., 2010; *Stap et al*., 2010; *Zachos et al*., 2010]. Warming during these hyperthermals was coeval

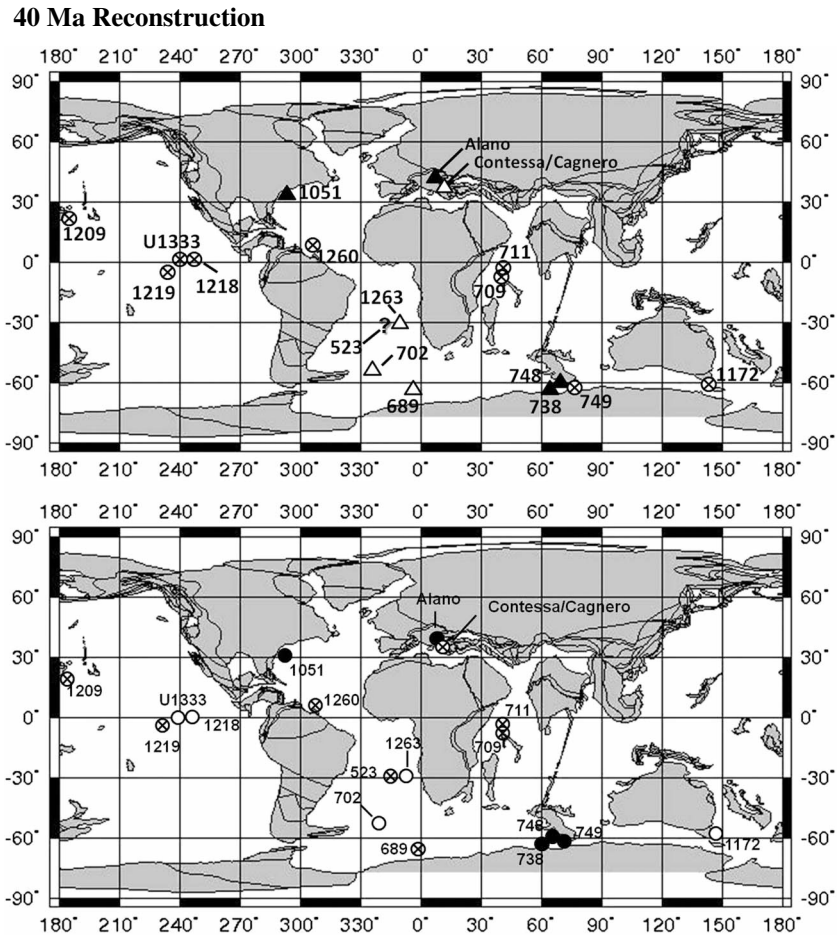

Figure 1. Drill sites and sections on land where the MECO has been described. Approximate positions at 40 Ma are plotted on a paleogeographic reconstruction from the Ocean Drilling Stratigraphic Network (GEOMAR, Kiel, Germany). (top) Sites where the negative CIE is well expressed are labeled with a solid triangle, sites with a doubtful CIE are labeled with an open triangle, and sites where no data are available are labeled with an open circle with a cross. (bottom) Sites with inferred increased productivity during the MECO are labeled with solid circles, sites with inferred decreased or unchanged productivity are labeled with open circles, and sites where no data are available are labeled with open circles with a cross.

with a negative carbon isotope excursion (CIE) and carbonate dissolution, indicative of ocean acidification [*Zachos et al*., 2005; *Lunt et al*., 2011; *Leon-Rodriguez and Dickens*, 2010; *McInerney and Wing*, 2011; *Hoenisch et al*., 2012; *Penman et al*., 2014], caused by a relatively rapid release of ^{13}C-depleted carbon [*Zachos et al*., 2005, 2008; *McInerney and Wing*, 2011; *Hoenisch et al*., 2012].

The MECO has been described as a global carbon cycle perturbation [*Bijl et al*., 2010], but the lack of a CIE contemporaneous with warming and the duration of the climate anomaly suggest that the event was more complex than the earlier hyperthermals [*Sluijs et al*., 2013]. There is no evidence for the release of isotopically light carbon coupled to MECO warming. Marine carbonate δ^{13}C records show considerable geographic and bathymetric variability but are usually characterized by rising rather than declining δ^{13}C values during the initial gradual warming [*Bohaty and Zachos*, 2003; *Bohaty et al*., 2009; *Borelli et al*., 2014]. A transient, ~0.5‰ negative CIE (~50 kyr) during peak warming occurs at some but not all sites (Figure 1) [*Bohaty et al*., 2009; *Edgar et al*., 2010; *Spofforth et al*., 2010]. Coeval with the MECO was a widespread, ~1 Myr long decrease in carbonate mass accumulation rate at water depths greater than 3000 m in the Indian and SE Atlantic Oceans [*Bohaty et al*., 2009].

In the equatorial Pacific, carbonate mass accumulation rates declined at sites at depths greater than 2000 m [*Hancock and Dickens*, 2005; *Bohaty et al*., 2009]. The carbonate compensation depth (CCD) shoaled from ~4100 to ~3200 m depth [*Pälike et al*., 2012], and the preservation of nannofossils decreased [*Toffanin et al*.,

2013], as the abundance of benthic foraminifera [*Takata et al*., 2013]. The MECO-associated CCD rise occurred within the 2 Myr interval between carbonate accumulation events CAE-3 and CAE-4 [*Lyle et al*., 2005, 2008; *Pälike et al*., 2012] and was one of several, similar CCD events superimposed on a longer-term trend of CCD deepening in the Pacific Ocean [*Pälike et al*., 2012].

Only a few studies have focused on the paleoenvironmental and paleobiotic consequences of the MECO. The event led to a significant crisis of muricate planktic foraminifera (acarininids and morozovelloids [*Luciani et al*., 2010; *Edgar et al*., 2013]) and temporary loss of photosymbionts (bleaching) in *Acarinina* [*Edgar et al*., 2013], possibly caused by the warming itself. Integrated studies of various microfossil and geochemical proxies in a western Tethys section deposited at middle-bathyal paleodepth [*Spofforth et al*., 2010; *Luciani et al*., 2010; *Toffanin et al*., 2011; *Boscolo Galazzo et al*., 2013] record higher export productivity during the MECO peak and directly afterward [*Boscolo Galazzo et al*., 2013]. At Site 1051 (NW Atlantic), diatoms and silicoflagellates increased in abundance during MECO initial warming, then decreased at peak MECO, while benthic foraminiferal data indicate an increase in delivery of organic matter to the seafloor [*Moebius et al*., 2013; *Witkowski et al*., 2014]. Siliceous phytoplankton also peaked in abundance at Southern Ocean Sites 748 and 749 (Indian Ocean sector [*Witkowski et al*., 2012]), with increased primary productivity supported by nannofossil data [*Villa et al*., 2014]. At Site 738 (Kerguelen Plateau), benthic foraminiferal assemblage data combined with a cerium anomaly suggest decreased bottom water oxygenation during peak warming, whereas productivity and export productivity increased during the entire event [*Moebius et al*., 2014]. Calcareous nannoplankton assemblages indicate eutrophic conditions at Southern Ocean Site 738 [*Villa et al*., 2014]. In contrast, dinocyst assemblages at Ocean Drilling Program (ODP) Site 1172, a marginal marine shelf area at southern high latitudes, indicate lower productivity [*Bijl et al*., 2010], consistent with interpretation of calcareous nannofossil assemblages at Site 702 (subpolar South Atlantic) during peak warming [*Pea*, 2011]. Pacific CAEs are argued to have been high-productivity events, as confirmed by tentative benthic foraminiferal data indicating increased delivery of organic matter to the seafloor [*Takata et al*., 2013], with the MECO reflecting a relatively low productivity interval at equatorial Pacific sites [*Lyle et al*., 2005, 2008]. Thus, there is clear evidence for substantial geographic differences in oceanic productivity during the event (Figure 1).

For this study, we generated stable oxygen and carbon isotopic records from bulk carbonate and benthic and planktic foraminifera at ODP Site 1263 on the Walvis Ridge in the midlatitude southeastern Atlantic Ocean [*Zachos et al*., 2004; *Bohaty et al*., 2009], in order to investigate the expression of the MECO throughout the water column. Sea surface temperature (SST) changes were estimated using the TEX_{86} proxy, because planktic foraminifera were recrystallized, compromising oxygen isotope values as commonly observed [*Pearson et al*., 2001; *Sexton et al*., 2006]. Carbon isotope records were used to infer changes in ocean stratification and compared with benthic foraminiferal accumulation rate (BFAR), a proxy for primary productivity in the absence of changes in delivery of organic matter to the seafloor [*Herguera and Berger*, 1991]. This study is one of the the first multiproxy investigations of the MECO in an open-ocean setting and aims to improve our understanding of this climatic perturbation and its paleoceanographic and paleoecological repercussions.

2. Location and Setting

ODP Site 1263 (28°53′S, 2°78′E, modern water depth 2717 m; ~800 km off the coast of Africa; Figure 1) was drilled during ODP Leg 208 on the north facing flank of Walvis Ridge (SE Atlantic Ocean [*Zachos et al*., 2004]). Site 1263 lies beneath the eastern part of the central subtropical gyre, outside the eastern boundary current with its associated high productivity. The seafloor at Site 1263 presently is bathed by Antarctic Intermediate Water, with North Atlantic Deep Water at slightly greater depths [*Klevenz et al*., 2008]. In the middle Eocene, Site 1263 was at a paleodepth of about 2000 m [*Zachos et al*., 2004] and likely bathed by a southern sourced, intermediate to deepwater mass [*Via and Thomas*, 2006; *Thomas and Via*, 2007; *Stap et al*., 2010; *Borelli et al*., 2014]. Eocene sediments are nannofossil ooze, foraminifer-bearing nannofossil ooze, clay-bearing nannofossil ooze, and chalky nannofossil ooze, with a low concentration of total organic carbon (0.86–0.00 wt %; mean = 0.09 wt % [*Zachos et al*., 2004]). Sediments vary in color between light gray and gray at decimeter scale and contain white, 1–4 cm "blebs" surrounded by dark haloes containing fine-grained, black to brown oxides [*Zachos et al*., 2004], which may be cross sections of burrows.

Site 1263 has a complete and relatively expanded record across the MECO, with an average linear sedimentation rate for the studied interval of 0.74 cm/kyr [*Bohaty et al*., 2009] and well-constrained nannofossil biostratigraphy [*Fornaciari et al*., 2010].

3. Methods

We generated bulk $CaCO_3$ stable isotopes and TEX_{86} data on 46 samples (Table S1 in the supporting information). The bulk isotope record has a 20 cm sample resolution within the MECO, 40 cm above and below. An additional set of 34 samples spaced at 40 cm was used for foraminiferal stable isotope analyses, accumulation rate, and planktic/benthic foraminifer calculations (Table S1 in the supporting information).

We used the relatively simple age model adopted by *Bohaty et al*. [2009], based on magnetobiostratigraphy and correlations to other sites using stable isotope records. We report data as a function of depth (meter composite depth (mcd)) and age [*Pälike et al*., 2006], at a resolution of ~25 kyr for the bulk record and ~50 kyr for foraminiferal records.

3.1. Stable Isotope Measurements

Samples were air dried and weighed, disaggregated in deionized water, and washed through sieves with mesh sizes of ≥38, ≥63, and ≥500 μm. The size fraction larger than 63 μm was weighed and split into two equal parts with a precision microsplitter. Benthic foraminiferal stable isotope records ($\delta^{13}C$ and $\delta^{18}O$) were generated for the epifaunal species *Nuttallides truempyi* [*Thomas and Shackleton*, 1996; *Katz et al*., 2003], following taxonomy by *van Morkhoven et al*. [1986]. Planktic foraminiferal stable isotope records ($\delta^{13}C$ and $\delta^{18}O$) were generated on mixed species of the surface-dwelling, photosymbiont-bearing genus *Acarinina* [*Pearson et al*., 2006]. The species *Acarinina topilensis* and *A. praetopilensis* were selected to limit interspecific variability, but this was not always possible due to the decrease in abundance of muricate planktic foraminifera during peak warming (139.4–137.4 mcd) and ~3–4 m higher.

Benthic and *Acarinina* stable isotope analyses were carried out on specimens from the size fraction between 250 and 180 μm in samples between 145 and 132 meter composite depth (mcd). We also generated a stable isotope record at 40 cm sample resolution for the mixed layer genus *Globigerinatheka* [e.g., *Pearson et al*., 2006] in the ≥500 μm size fraction for the 145–136 mcd interval.

Bulk $CaCO_3$ stable isotopes were measured for the interval between 147 and 132 mcd. Bulk and foraminiferal samples were analyzed for stable oxygen and carbon isotopes by acid digestion using an individual vial acid drop ThemoScientific Kiel IV carbonate device interfaced to Thermo Scientific MAT-253 dual-inlet isotope ratio mass spectrometer (IRMS) at the University of California, Santa Cruz. Samples were reacted at 75°C in orthophosphoric acid (specific gravity = 1.92 g/cm^3) to generate carbon dioxide and water. During this procedure, water was cryogenically removed from CO_2, and noncondensable gases are pumped away, prior to the introduction of the purified CO_2 into the IRMS. A calibrated, in-house standard of Carrara Marble was used to correct analytical offsets. Four NBS-18 limestone standards were used in conjunction with Carrara Marble to correct for instrument-specific source ionization effects. NBS-19 standards were used to monitor quality control and long-term performance. Carrara Marble has been extensively calibrated against National Institute of Standards and Technology Standard Reference Materials (NBS-19, NBS-18, and LSVEC) and as part of intercomparison studies with other stable isotope laboratories. Sets of standards were run before and after running the samples; analytical precision is estimated at 0.04‰ for $\delta^{13}C$ and 0.06‰ for $\delta^{18}O$. Corrected delta values are expressed relative to international standards Vienna Peedee belemnite for $\delta^{13}C$ and $\delta^{18}O$.

To compare our records with those in *Bohaty et al*. [2009], oxygen isotope values were converted to paleotemperatures using the equation of *Shackleton* [1974], assuming a global mean $\delta^{18}O$ for seawater ($\delta^{18}O_{sw}$) of −1.0‰, representing an ice-free world [*Zachos et al*., 1994; *Huber et al*., 2003; *Burgess et al*., 2008; *Bohaty et al*., 2009], although the presence of small continental ice sheets on Antarctica cannot be ruled out [*Tripati et al*., 2005; *Edgar et al*., 2007; *Dawber and Tripati*, 2011; *Bohaty et al*., 2009].

3.2. Tetraether Lipid Analysis

Samples were processed and analyzed for glycerol dialkyl glycerol tetraether (GDGT) lipids in the Organic Biogeochemistry and Paleoclimatology Laboratory at Yale University following *Schouten et al*. [2002, 2013]. Compounds were extracted from freeze-dried sediment samples with a soxhlet extractor using a 2:1 dichloromethane:methanol solvent mixture. The lipid extracts were then separated into apolar, ketone, and polar fractions via silica gel column chromatography. GDGTs were further purified via alumina chromatography and filtered through 0.45 μm glass fiber filters. Quantification of GDGTs was conducted

using high-performance liquid chromatography–atmospheric pressure chemical ionization mass spectrometry (HPLC-APCI-MS; Agilent1200 series liquid chromatograph and Agilent 6130 series single quadrupole mass spectrometer), following *Schouten et al*. [2007]. A Prevail Cyano column was used with 99:1 hexane:isopropanol as eluent. The solvent gradient was 100% hexane/isopropanol (99:1, vol/vol; 5 min), then increasing the amount of hexane/isopropanol at a ratio of 90:10 vol/vol (0% at 5 min to 7.4% at 40 min; held 10 min). Samples were scanned in selected ion monitoring mode. Peak integration was carried out using Agilent Chemstation. Analytical precision is estimated at ±0.01 TEX_{86} units.

TEX_{86} values were calculated using the equation of *Schouten et al*. [2002]:

$$TEX_{86} = [GDGT2 + GDGT3 + cren']/[GDGT1 + GDGT2 + GDGT3 + cren'] \quad (1)$$

where GDGTs 1–3 indicate compounds containing 1–3 cyclopentyl moieties, and cren′ denotes the regioisomer of crenarchaeol.

Several TEX_{86} temperature calibrations have been derived [e.g., *Pearson and Ingalls*, 2013]. *Kim et al*. [2010] recommend the use of the TEX_{86}^{H} for SSTs >15°C, implying that it would be appropriate for the middle Eocene subtropics, but *Hollis et al*. [2012] show the best fit among Eocene low-latitude SSTs derived from carbonate proxies and >0.85 TEX_{86} values with *Liu et al*.'s [2009] calibration. Accordingly, we apply both the high-temperature logarithmic calibration of *Kim et al*. [2010]:

$$SST = 68.4[\log(TEX_{86})] + 38.6 \quad (2)$$

and the nonlinear calibration of *Liu et al*. [2009]:

$$SST = 50.475 - 16.332(1/TEX_{86}) \quad (3)$$

to estimate SST change during the MECO.

We also applied the Bayesian calibration model (Bayesian Spatially Varying Regression) "deep time" version developed by *Tierney and Tingley* [2014]. Relative to prior TEX_{86} calibrations, the Bayesian model propagates calibration uncertainty and allows model parameters to vary spatially.

The Branched and Isoprenoid Tetraethers Index, a proxy for terrestrial organic matter input, was calculated following *Hopmans et al*. [2004] in order to evaluate the influence of terrestrial organic matter input that arguably biases TEX_{86} temperature estimates:

$$BIT = [I + II + III]/[I + II + III] + IV \quad (4)$$

where compounds I, II, and III represent the branched GDGTs derived from soil bacteria and compound IV is crenarchaeol, an isoprenoidal GDGT primarily derived from marine archaea, a compound distinct from the crenarchaeol regioisomer used in the calculation of TEX_{86}.

3.3. Foraminiferal and Fine Fraction Accumulation Rates

The benthic foraminiferal accumulation rate (BFAR) was calculated from the numbers in representative splits of the size fraction ≥63 μm containing ≥400 specimens, corrected to the weight of bulk sediment. The BFAR is a proxy for total organic matter flux reaching the seafloor [e.g., *Gooday*, 2003; *Jorissen et al*., 2007], because benthic foraminifera rely on the organic matter produced in the surface and exported down in the water column. Organic flux reaching the seafloor is a function of primary productivity and remineralization of organic matter in the water column [e.g., *Henson et al*., 2011; *Arndt et al*., 2013; *Ma et al*., 2014]. We calculated the coarse fraction as the weight ratio of the dry ≥63 μm size fraction to the bulk dry sediment weight. The fine fraction was calculated as the weight ratio of the bulk dry sediment minus the coarse fraction weight to the bulk dry sediment. Coarse and fine fraction accumulation rates (CFAR and FFAR) were calculated using linear sedimentation rates and dry bulk density. Linear sedimentation rates were derived using the age model of *Bohaty et al*. [2009]. Dry bulk density was estimated by extrapolating the density values for the studied interval [*Zachos et al*., 2004], which show little variability. The benthic foraminiferal accumulation rate (BFAR) was calculated following *Herguera and Berger* [1991]:

$$BFAR\left(\text{number of specimens } cm^{-2}kyr^{-1}\right) = N/g * LSR * DBD \quad (5)$$

where N/g is the number of benthic foraminifera per gram dry bulk sediment, LSR is the linear sedimentation rate (cm/kyr), and DBD is the dry bulk density (g/cm^3).

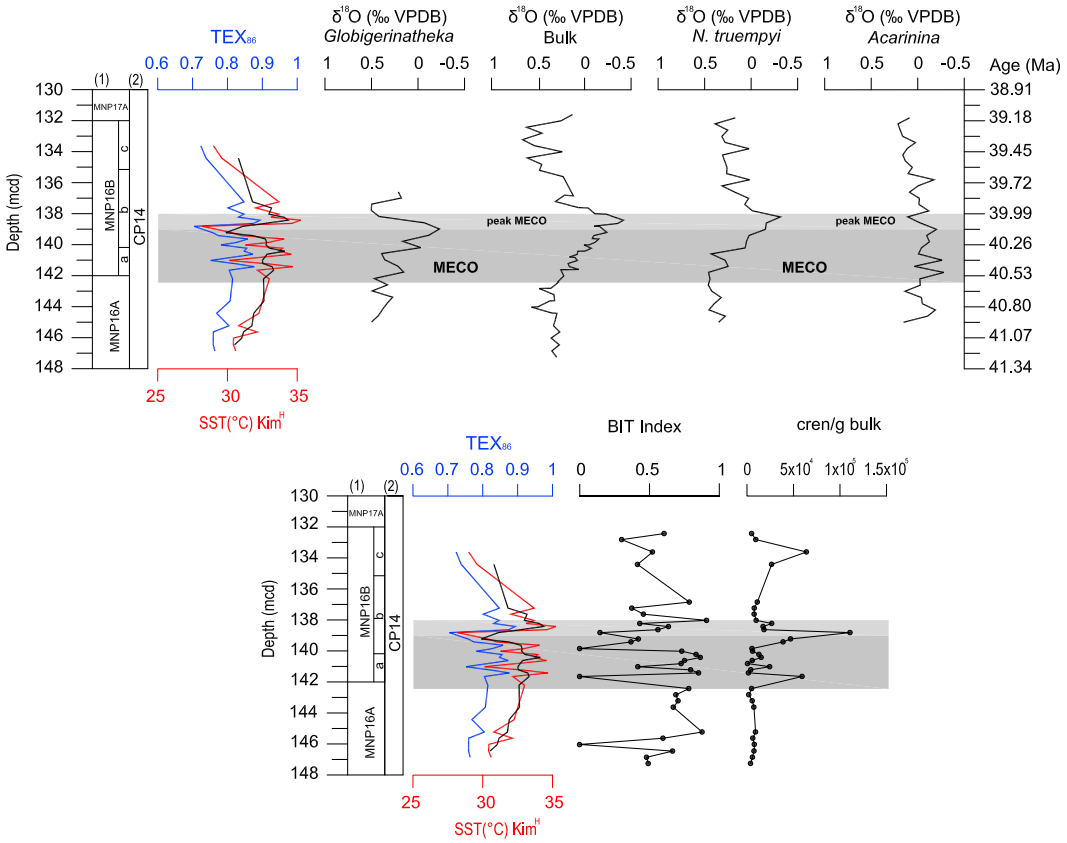

Figure 2. (top) ODP Site 1263 TEX_{86} and $\delta^{18}O$ data plotted versus meter composite depth. The black line in the TEX_{86} SST plot is the three-point running mean. (bottom) TEX_{86}, BIT indices and cren/g bulk plotted versus meter composite depth. The black line in the TEX_{86} SST plot is the three-point running mean. Cren/g bulk is the abundance of the biomarker crenarchaeol from peak area integrations normalized to the weight of bulk sediment. The area shaded in gray highlights the entire MECO interval, with light gray indicating the peak of the MECO. Biostratigraphy after *Fornaciari et al.* [2010] following (1) calcareous nannofossil zonation of *Fornaciari et al.* [2010] and (2) nannofossil standard zonation of *Okada and Bukry* [1980]. Age model after *Bohaty et al.* [2009].

We used CFAR as an approximation of the planktic foraminiferal accumulation rate, because this fraction dominantly consists of planktic foraminifera in pelagic sediments not significantly affected by dissolution [*Diester-Haass*, 1995]. In typical oceanic calcareous oozes dominated by calcareous nannofossils, FFAR can, with some caution, be considered indicative of the calcareous nannofossil accumulation rate.

We calculated the planktic/benthic foraminiferal value (P/(P + B)%, briefly P/B), an indicator of carbonate dissolution [*Berger and Diester-Haass*, 1988] expressed as the proportion of planktic specimens in the total foraminiferal assemblage (≥63 μm fraction), for each sample across the MECO and in some samples below and above, counting a consistent number of planktic foraminiferal tests (600–630).

4. Results

4.1. Oxygen Isotope Records

The negative $\delta^{18}O$ excursion typical for the MECO is present in the benthic, bulk, and *Globigerinatheka* records. In contrast, the *Acarinina* record does not show a $\delta^{18}O$ excursion, but above 136.8 mcd, values slightly increase to the top of the studied section (Figure 2). *Globigerinatheka* $\delta^{18}O$ values decrease upward from the base (145 mcd). The lowest *Globigerinatheka* $\delta^{18}O$ values occur at 139.6–138.4 mcd for a total excursion of −0.9‰ (~4°C), from 0.4 to −0.5‰, and recover to preexcursion values within 40 cm (138.4–138 mcd) corresponding to ~50 kyr (Figure 2).

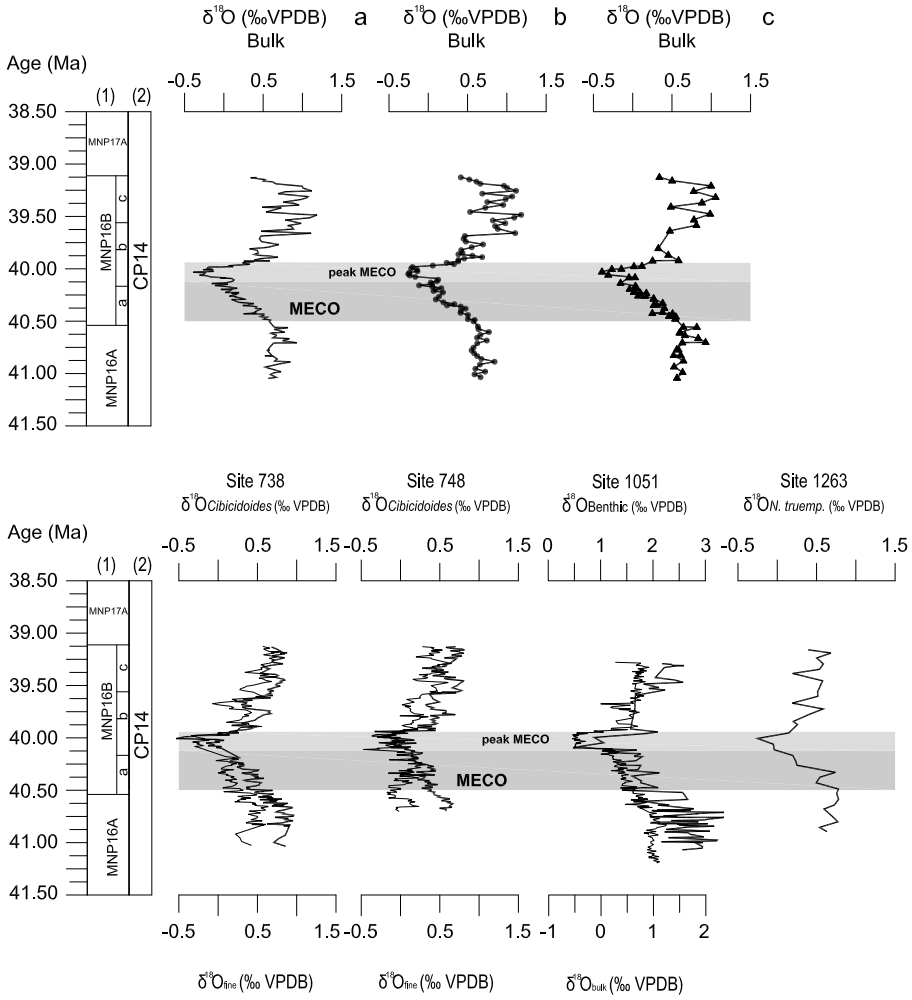

Figure 3. (top) Site 1263 bulk carbonate $\delta^{18}O$ data plotted versus numerical age. (a) Bulk $\delta^{18}O$ data generated in the present study combined with bulk data in *Bohaty et al.* [2009]. (b) Bulk isotope data from *Bohaty et al.* [2009]. (c) Bulk isotope data generated in this study. (bottom) Compilation of benthic $\delta^{18}O$ records for the MECO plotted versus numerical age and compared with bulk/fine fraction records from the same sites (thinner lines). Sites 738 and 748 data are from *Bohaty et al.* [2009], Site 1051 data are from *Bohaty et al.* [2009], and *Edgar et al.* [2010] aligned on the *Bohaty et al.*'s [2009] age model. Biostratigraphy after *Fornaciari et al.* [2010] following (1) calcareous nannofossils zonation of *Fornaciari et al.* [2010] and (2) nannofossil standard zonation of *Okada and Bukry* [1980]. Age model after *Bohaty et al.* [2009].

Our bulk $\delta^{18}O$ data closely match those from *Bohaty et al.* [2009] (Figure 3), with stable values around 0.5‰ from the base (147 mcd; 41.2 Ma) up to ~142.60 mcd. Values gradually decrease up to ~139 mcd, where a sharp negative ~0.4‰ $\delta^{18}O$ shift is recorded. Minimum values occur at 138.7–138.1 mcd, and the overall excursion is −1‰ (corresponding to 4°C; Figure 4). The $\delta^{18}O$ values rapidly recover, reaching preevent values at 137.4 mcd, 70 cm (~100 kyr) above the minimum value. Between 137.3 and 136 mcd, bulk $\delta^{18}O$ values start to gradually increase up to the top of the studied interval (Figures 2–4). *Nuttallides truempyi* $\delta^{18}O$ values are stable, varying around 0.6‰ from the base of the record up to ~140.8 mcd, and then markedly decrease with a minimum between 138.4 and 138 mcd, and reaching a total excursion of −0.9‰ (Figures 2 and 3). The recovery starts at 138 mcd, reaching preexcursion values by ~136 mcd, 200 cm (270 kyr) above peak MECO (Figures 2, 3, and 4). In total, a deepwater temperature increase of 4°C is estimated from ~9.5 to ~13.5°C (Figure 4).

A similar decrease in $\delta^{18}O$ values is recorded in benthic, bulk, and *Globigerinatheka* records (Figures 2 and 4), but the main phases of the MECO (i.e., onset, peak warming, and termination) occur at slightly different depths. Changes in the *Globigerinatheka* record occur lowest, followed by up-section of those in the bulk and the *N. truempyi* record (Figure 2). In addition, the MECO and peak warming occur over a thinner core section

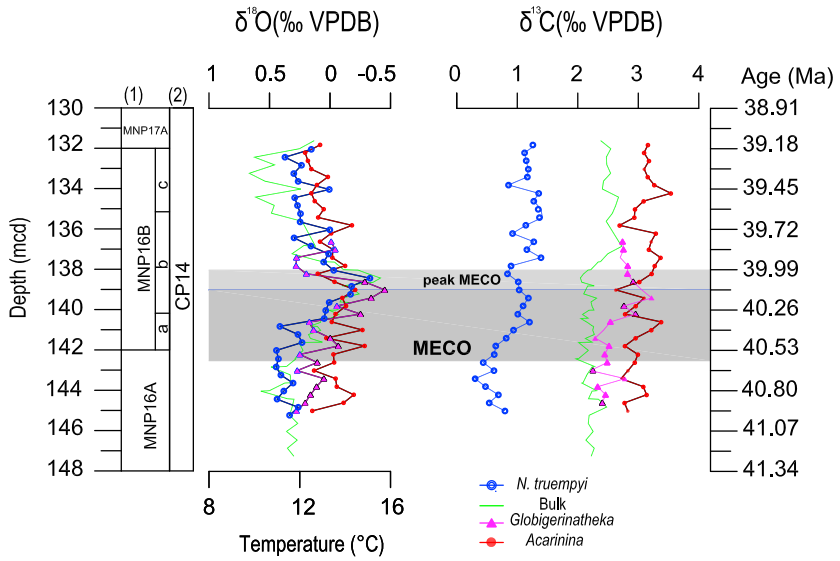

Figure 4. ODP Site 1263 oxygen and carbon isotope records plotted versus meter composite depth. The $\delta^{18}O$ axis is inverted to give a positive temperature increase in the upward direction. Biostratigraphy after *Fornaciari et al.* [2010] following (1) calcareous nannofossil zonation of *Fornaciari et al.* [2010] and (2) nannofossil standard zonation of *Okada and Bukry* [1980]. Age model after *Bohaty et al.* [2009].

(i.e., equivalent to a shorter duration) in the benthic and bulk carbonates than in the *Globigerinatheka* record. Recovery to preexcursion values is sharp in the *Globigerinatheka* record, whereas bulk and *N. truempyi* records show a more gradual recovery (Figure 2). The shape of the benthic $\delta^{18}O$ excursion appears more symmetrical than those in planktic and bulk-carbonate records (Figure 2).

Below the MECO, values and patterns in bulk and benthic foraminiferal $\delta^{18}O$ are very similar (Figures 2–4), but bulk values above MECO are higher than in *N. truempyi*.

Globigerinatheka yields generally slightly lower values than both *N. truempyi* and bulk (Figures 2 and 4).

Globigerinatheka is a symbiont-bearing mixed layer dweller [*Pearson et al.*, 1993; *Pearson et al.*, 2001; *Wade and Kroon*, 2002], but stable isotope values commonly indicate calcification in deeper waters [*Wade*, 2004; *Sexton et al.*, 2006; *Premoli Silva et al.*, 2006; *Burgess et al.*, 2008, present study] (Figures 2 and 4), suggesting that the genus had late-stage calcification, with $CaCO_3$ crusts forming deeper in the water column [*Pearson et al.*, 2001; *Premoli Silva et al.*, 2006]. *Globigerinatheka* isotope records thus reflect conditions between the mixed layer and the thermocline [*Boersma et al.*, 1987; *Wade*, 2004; *Sexton et al.*, 2006], as also indicated by boron isotope data [*Pearson and Palmer*, 2000]. *Acarinina*, a photosymbiont-bearing genus calcifying within the mixed layer, has somewhat more negative $\delta^{18}O$ values above and below the MECO interval, but across MECO, its values overlap with the *Globigerinatheka*, bulk, and *N. truempyi* records because of the lack of an excursion (Figures 2 and 4).

4.2. TEX_{86} Record and BIT Index

Isoprenoidal GDGTs containing cyclopentane rings are in low abundance over the studied interval. Despite the analysis of large (50 cm^3) samples, only 29 of the 46 samples analyzed had concentrations above the detection limit. Concentrations in samples between 147 and 143 mcd and from 138 mcd to the top of the studied interval were generally below detection, but the abundance of marine isoprenoidal GDGTs was somewhat higher between 142 and 138 mcd, coincident with the MECO (Figure 2).

Using the high-temperature calibration of *Kim et al.* [2010], TEX_{86} values of ~0.76 between 147 and 145.22 mcd imply a mean surface temperature of ~30.5°C (Figure 2). A gradual up-section increase in TEX_{86} values by 0.2 occurs between ~144.8 mcd and 142 mcd, implying warming from 30.5 to 33°C (Figure 2). From 141.5 mcd upward, TEX_{86}-SSTs show an abrupt increase of 1°C. This interval displays strong fluctuations with a large decrease (from 0.85 to 0.7) between ~140 and 138.7 mcd and a rapid recovery to the highest temperature recorded (~34.5°C) between 138.7 and 138.3 mcd, followed by a rapid decrease to 29°C (Figure 2).

Our data indicate a maximum SST excursion of 4.5°C (Figure 2) using TEX_{86}^{H}. The use of the calibration of *Liu et al*. [2009] results in the same trend, but lower overall temperatures and less warming (3°C, from background 29 to 32°C at peak warmth), although this temperature difference is within the calibration error of our data [*Liu et al*., 2009; *Kim et al*., 2010]. SSTs derived from the Bayesian regression model as well as the shape and magnitude of MECO temperature excursion are very close to those derived from the other two calibrations (range of uncertainty is ±2–3°C).

TEX_{86}-derived SSTs are much higher than those estimated from planktic $\delta^{18}O$ values (~14°C), although the magnitude of the temperature excursion is similar. Surface temperatures are considerably higher than those reported for Eocene Thermal Maximum 2 from a single TEX_{86} data point integrated over 35 cm of sediment at Site 1263 (~25°C [*Stap et al*., 2010], using both *Kim et al*.'s [2010] and *Liu et al*.'s [2009] calibrations).

Branched and isoprenoid tetraether (BIT) indices are very high in all samples, with a maximum of 0.8 (mean 0.55; Figure 2). Such high values are usually found in coastal environments close to fresh water influx carrying terrestrially derived organic matter [*Hopmans et al*., 2004; *Smith et al*., 2012]. A BIT index >0.3 has been used to imply that TEX_{86} temperature estimates are compromised by the presence of soil-derived isoprenoidal GDGTs [*Weijers et al*., 2006]. However, Site 1263 is in an open-ocean setting ~800 km from land [*Moore et al*., 1984], and therefore, it appears unrealistic that high BIT values represent a substantial amount of riverine-delivered organic matter.

Aeolian dust can carry soil-derived GDGTs to open-ocean areas, but odd numbered long-chain *n*-alkanes are usually more abundant than GDGTs in dust samples [*Fietz et al*., 2013]. Long chain *n*-alkanes with odd-over-even carbon predominance, indicative of a terrestrial higher plant origin, are below detection limit in all of our samples. In addition, BIT index values and TEX_{86} are not significantly correlated ($R^2 = 0.1763$; Figure S1 in the supporting information) [*Huguet et al*., 2009]. High BIT indices could possibly be explained by a greater preservation potential of branched GDGTs. In oxidized marine sediments, isoprenoidal GDGTs have lower preservation efficiency than terrestrially derived branched GDGTs, and their preferential degradation increases BIT indices without affecting TEX_{86} values [*Huguet et al*., 2009; *Lengger et al*., 2013]. Alternatively, in situ production of branched GDGTs in marine sediments is possible [*Peterse et al*., 2009; *Zhu et al*., 2011; *Fietz et al*., 2012; *Hu et al*., 2012; *Lengger et al*., 2013].

Accordingly, we suggest that the locality of Site 1263 and the lack of higher plant leaf waxes argue against the influence of terrestrially derived GDGTs on our TEX_{86}-derived temperatures and assume that TEX_{86} SST estimates are robust, particularly the SST trends.

4.3. Carbon Isotope Records

The *Acarinina* $\delta^{13}C$ record, similar to its $\delta^{18}O$ record, shows variability without a trend (Figure 4). *Globigerinatheka* $\delta^{13}C$ values vary (−0.2‰) from the start of the event to ~142 mcd around an average value of 2.5‰, then increase from ~141.4 mcd upward until ~139.5 mcd, with peak values of 3‰, coinciding with the lowest $\delta^{18}O$ values. The $\delta^{13}C$ values decrease above this level but remain higher than the preevent values (Figure 4). Our bulk $\delta^{13}C$ data closely match with the data of *Bohaty et al*. [2009] (Figure 5). Bulk $\delta^{13}C$ values show minor (~0.2‰) variability around a mean value of 2.2‰ from the onset of the MECO to 137.8 mcd, coinciding with minimum $\delta^{18}O$ values (Figures 4 and 5). At 137.8 mcd, bulk $\delta^{13}C$ values increase up-section by about 0.5‰, then remain stable throughout the studied interval (Figures 4). Benthic $\delta^{13}C$ values are ~1.5‰ lower than bulk $\delta^{13}C$ values and increase from ~144 to ~141 mcd, then remain stable, with a small decline at ~138 mcd, the top of the MECO interval with the most negative $\delta^{18}O$ values. The $\delta^{13}C$ values increase up-section and then remain stable up to the top of the studied interval, fluctuating around 1.2 ‰ (Figures 4 and 5).

Overall, $\delta^{13}C$ records of *Globigerinatheka*, benthic, and bulk gradually become more positive upward in the section (Figures 4 and 5; see also Figure 5 in *Borelli et al*. [2014]). The $\delta^{13}C$ increase coincides with the negative oxygen isotope excursion in benthic and *Globigerinatheka* records, whereas the increase starts above the MECO interval in the bulk record. In contrast to other sites (e.g., Southern Ocean Sites 738 and 748 [*Bohaty et al*., 2009]) (Figure 5), a brief negative CIE coinciding with peak warming (minimum in the $\delta^{18}O$ records) is lacking at Site 1263, although bulk and benthic records show a minor decrease in $\delta^{13}C$ values at the top of the MECO interval (~138 mcd; Figures 4 and 5).

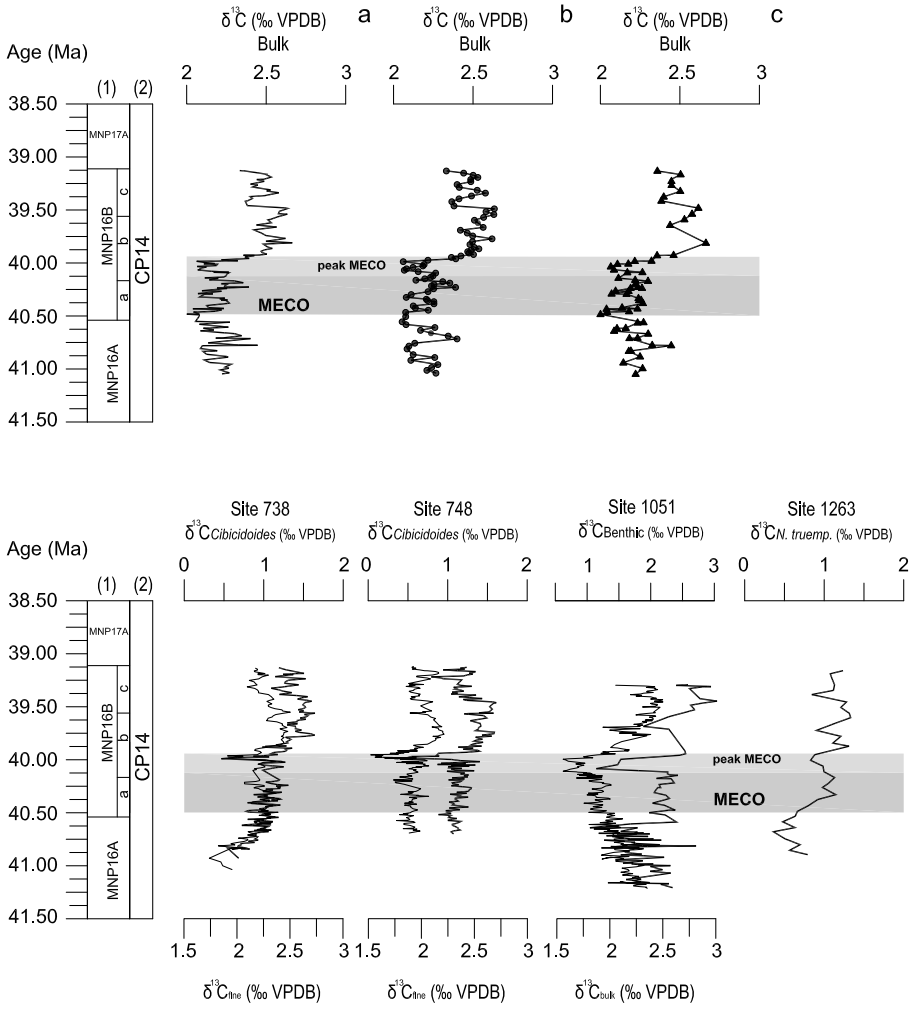

Figure 5. (top) Site 1263 bulk carbonate $\delta^{13}C$ data plotted versus numerical age. (a) Bulk $\delta^{13}C$ data generated in this study combined with bulk $\delta^{13}C$ data in *Bohaty et al.* [2009]. (b) Bulk isotope data from *Bohaty et al.* [2009]. (c) Bulk isotope data generated in this study. (bottom) Compilation of benthic $\delta^{13}C$ data for the MECO interval plotted versus numerical age and compared with bulk/fine fraction records from the same sites (thinner lines). Sites 738 and 748 data are from *Bohaty et al.* [2009], Site 1051 data are from [*Bohaty et al.*, 2009], and *Edgar et al.* [2010] aligned on *Bohaty et al.* [2009] age model. Biostratigraphy after *Fornaciari et al.* [2010] following (1) calcareous nannofossils zonation of *Fornaciari et al.* [2010] and (2) nannofossil standard zonation of *Okada and Bukry* [1980]. Age model after *Bohaty et al.* [2009].

4.4. Foraminiferal and Fine Fraction Accumulation Rates

Benthic foraminiferal (BFAR) and coarse fraction (CFAR; i.e., planktic foraminifera) accumulation rates covary throughout the studied interval. From the base of the studied interval, both CFAR and BFAR increase, reaching peak values at about 142–141 mcd. Values then decrease up-section, reaching a minimum at about 139 mcd, the interval of peak MECO warming. Above this interval, values remain relatively stable (Figure 6). Fine fraction accumulation rate (FFAR) values vary throughout the studied interval without a discernible trend (Figure 6). The P/B remains constant throughout the studied interval (mean 97%), with fluctuations across MECO in the range of 1–2% (Figure 6).

5. Discussion

5.1. Temperature Anomaly

The planktic foraminiferal assemblage at Site 1263 appears moderately well preserved but with tests exhibiting "frosty" preservation [*Sexton et al.*, 2006]. Frosty foraminifera are known to be affected by diagenesis, and their $\delta^{18}O$ values reflect partial recrystallization (as defined, e.g., in *Pearson et al.* [2001], *Sexton et al.* [2006], and

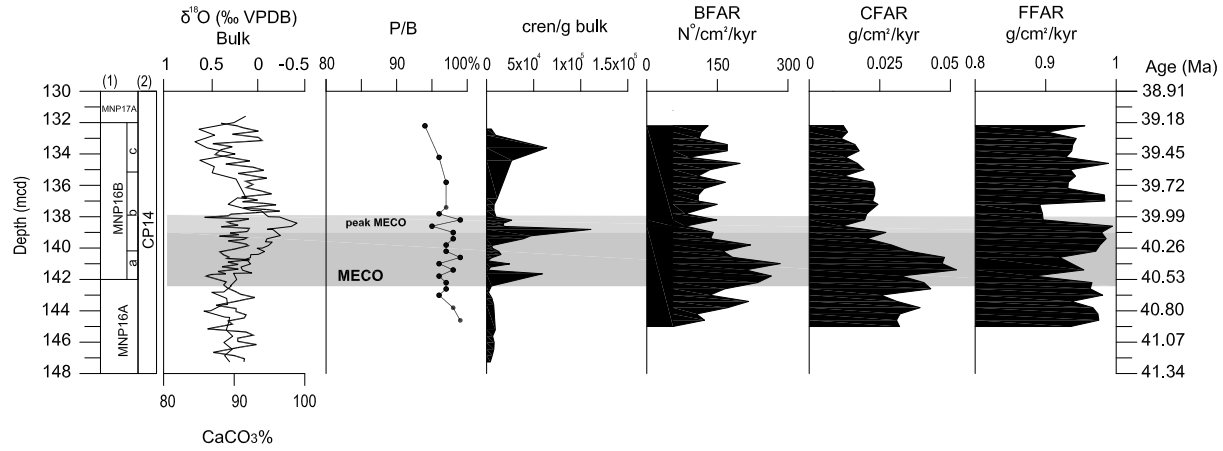

Figure 6. ODP Site 1263 bulk carbonate percentage (bold line) and $\delta^{18}O$ (thin line), planktic/benthic foraminiferal value (P/B), cren/g bulk, benthic foraminiferal, coarse fraction, and fine fraction accumulation rates (BFAR, CFAR, and FFAR) plotted versus meter composite depth. Cren/g bulk is the abundance of the biomarker crenarchaeol from peak area integrations normalized to the weight of bulk sediment. $CaCO_3$% from *Bohaty et al.* [2009]. Biostratigraphy after *Fornaciari et al.* [2010] following (1) calcareous nannofossil zonation of *Fornaciari et al.* [2010] and (2) nannofossil standard zonation of *Okada and Bukry* [1980]. Age model after *Bohaty et al.* [2009].

Pearson [2012]) at seafloor temperatures, which are much lower than those in the surface waters where the foraminifera calcified [e.g., *Schrag et al.*, 1995; *Pearson et al.*, 2001; *Stap et al.*, 2010; *Kozdon et al.*, 2011].

Carbonate oozes at Walvis Ridge consist primarily of calcareous nannofossils, as shown by the very high FFAR relative to CFAR (Figure 6). Accordingly, bulk isotopic records should primarily reflect signals of the lower photic zone where these organisms dominantly calcify [*Stoll*, 2005; *Stap et al.*, 2009]. Before the MECO, the vertical water column temperature gradient based on bulk, mixed layer dwelling *Acarinina*, the subsurface dweller *Globigerinatheka*, and benthic (~2000 m) $\delta^{18}O$ values apparently was ~2–3°C (Figure 4), even less than the gradient calculated for Eocene Thermal Maximum 2 (ETM2) at Site 1263 (~4°C [*Stap et al.*, 2010]). This gradient is much lower than today (~15°C [*Levitus et al.*, 1994]) and lower than in the warm Eocene oceans [*Huber and Thomas*, 2008]. Deepwater temperature estimates from benthic foraminifera are similar to bulk values from high-latitude Site 689 in the Weddell Sea [*Bohaty et al.*, 2009], which reflect the temperature of upper ocean waters in the region of deepwater formation [e.g., *Huber and Thomas*, 2008]. At ~41 Ma, just prior to the MECO, high latitudes cooled [*Tripati et al.*, 2005], whereas low latitudes probably remained warm, with surface water temperatures around 30–35°C [*Pearson et al.*, 2007]. Thus, we conclude that our planktic foraminiferal $\delta^{18}O$ data cannot be used to approximate mixed layer temperatures [*Pearson et al.*, 2001].

The *Acarinina*-derived temperatures (mixed layer) appear to be most compromised, lacking a negative $\delta^{18}O$ excursion during the MECO. This is not surprising, because *Acarinina* tests are more porous and thus more readily recrystallized than those of *Globigerinatheka* [*Pearson et al.*, 2001; *Sexton et al.*, 2006] (see also Figure S2 in the supporting information). In addition, *Acarinina* were less abundant during MECO [*Luciani*, unpublished data, 2014], so the lack of a $\delta^{18}O$ excursion in analyses of multiple specimens might in part be caused by bioturbational mixing of preevent and postevent specimens, as commonly observed during the Palaeocene–Eocene Thermal Maximum (PETM) [*Kelly et al.*, 1996].

The lack of a $\delta^{18}O$ excursion might possibly also be explained by the migration of *Acarinina* during MECO to greater depths, without losing its symbionts, thus keeping its carbon isotopic composition unchanged. Remaining at constant depth but losing symbionts [e.g., *Edgar et al.*, 2013] could explain the absence of a positive excursion in $\delta^{13}C$ during MECO (similar to that in *Globigerinatheka*) but not the lack of a negative oxygen isotope excursion. We thus conclude that the lack of oxygen isotope excursion in *Acarinina* most likely was due to recrystallization, as commonly observed [*Pearson et al.*, 2001], possibly combined with bioturbation.

Globigerinatheka $\delta^{18}O$ values are likely influenced by late ontogenetic (possibly gametogenic) calcite crusts [*Sexton et al.*, 2006], but the relatively positive $\delta^{18}O$ values in our records cannot be completely explained by depth habitat [*Hollis et al.*, 2012] also suggesting diagenetic alteration.

TEX_{86} estimates suggest background SSTs of ~30°C (Figure 2), significantly higher (9–6°C) than the present-day mean annual and summer temperature at the same latitude (~21–24°C [*Levitus et al*., 1994]), but consistent with middle to late Eocene SST records for middle to low latitudes [*Pearson et al*., 2007; *Liu et al*., 2009; *Zhang et al*., 2013]. The TEX_{86} record indicates surface water warming between 143 and 138 mcd, corresponding to the MECO interval [*Bohaty et al*., 2009] (Figure 2). This record, however, shows an earlier onset of warming (Figure 2), not expressed in $\delta^{18}O$ records [*Bohaty et al*., 2009] (Figure 2). TEX_{86} SSTs are high in the MECO interval but show large fluctuations (Figure 2). These fluctuations might be explained by the ecology of marine Thaumarchaeota, specifically variation in the location of maximum production relative to the thermocline and the chemocline [*Pearson and Ingalls*, 2013]. On the other hand, the fluctuations in the record might be at least partially explained by bioturbation. Calcareous nannofossil data from the same cores do not suggest evidence of reworking/contamination of the fine fraction due to pervasive bioturbation [*Fornaciari et al*., 2010], but the sediments may have been disturbed heterogeneously by large burrowers, with some samples possibly representing vertical burrows (halos [*Zachos et al*., 2004]). Bioturbation would affect the TEX_{86} record differently than the bulk stable isotope records because of the difference in isoprenoidal GDGT concentrations within/without the MECO and the difference in magnitude of the excursion in TEX_{86} and stable isotopes.

There is a similar uncertainty about primary signal and bioturbation in the explanation of the apparent offsets in the timing of warming by TEX_{86} and $\delta^{18}O$ records. Upper water column indicators (*Globigerinatheka* and TEX_{86}) consistently record the phases of the MECO lower in the sediment than deeper water indicators (bulk and benthic records; Figure 2). An earlier beginning and longer duration of the peak warming phase in the bulk than in the benthic record (Figure 2) were also observed by *Bohaty et al*. [2009] at Sites 738 and 748 (Figure 3), and a slower recovery in the benthic record (Figure 2) is evident at Site 1218 in the equatorial Pacific and at sites in the Southern Ocean (Figure 3) [*Lear et al*., 2004; *Tripati et al*., 2005; *Bohaty et al*., 2009]. These offsets could reflect actual differences in timing of the phases of the MECO (onset, peak warming, and termination), with a progressive delay of the onset from surface to deeper water (Figure 2), as has been suggested, though not generally accepted, for the PETM [*Thomas et al*., 2002; *Sluijs et al*., 2007; *Thomas*, 2003; *Dunkley-Jones et al*., 2013]. However, they may also represent bias due to differential bioturbation and/or diagenesis. For instance, GDGTs are associated with the fine-grained sediment fraction [*Shah et al*., 2008] and can be more easily bioturbated downward than larger particles [*Thompson et al*., 1995], although the difference between the age of fine-grained sediments and foraminifera is usually only ~1 kyr, i.e., much shorter than differences observed here. Whether or not differential bioturbation can account for the appearance of an earlier onset of warming in the TEX_{86} record (350 kyr earlier or 2.5 m below) remains speculative. This is the first study coupling planktic stable isotope, benthic stable isotope, and organic proxy temperature data sets for the MECO, so no other comparisons are available.

The ~4°C warming in surface and deeper waters (Figures 2 and 4) in our records is similar to that at other sites [*Bohaty and Zachos*, 2003; *Bohaty et al*., 2009; *Bijl et al*., 2010]. Uniform warming of the water column suggests that Southern Ocean surface waters, the probable source of Atlantic intermediate and deep waters [*Via and Thomas*, 2006; *Thomas and Via*, 2007; *Borelli et al*., 2014], warmed to a similar degree as the midlatitude surface waters. Polar amplification during the MECO was thus probably negligible, at least for southern high latitudes [*Intergovernmental Panel on Climate Change*, 2001; *Holland and Bitz*, 2003].

5.2. Repercussions of MECO Warming on Marine Food Webs and Transfer of Organic Carbon to the Seafloor

Globigerinatheka $\delta^{13}C$ values show a progressive increase approaching the peak warming of the MECO that is not apparent in the bulk $\delta^{13}C$ record (Figure 4). Such an increase can result from increased symbiont photosynthetic activity [e.g., *Spero and Williams*, 1988] and/or reflect lower seawater pH [*Spero et al*., 1997; *Birch et al*., 2013; *Penman et al*., 2014], possibly caused or exacerbated by enhanced water column remineralization of organic matter during warming [*John et al*., 2013; *Ma et al*., 2014]. Overall, $\delta^{13}C$ records at Site 1263 indicate well-developed water column stratification without substantial changes over the studied time period (Figure 4).

Benthic foraminifera and coarse fraction accumulation rates (BFAR and CFAR) increase at the beginning of the record, just below the MECO and up to the basal part of the bulk $\delta^{18}O$ negative excursion, then rapidly

decrease, with the lowest rates during peak warming (Figure 6). Our records do not extend sufficiently below the MECO to evaluate whether the increase at the beginning of the record is linked to the gradual warming phase of MECO.

The decrease in BFAR during the upper MECO suggests that the amount of organic matter arriving at the seafloor at Site 1263 declined. A parallel decrease in CFAR (Figure 6) could indicate a concomitant decrease in planktic foraminiferal productivity or carbonate dissolution. There is no significant decrease in $CaCO_3$% during MECO at Site 1263 [*Bohaty et al*., 2009] (Figure 6), and foraminiferal preservation does not show significant changes. In addition, the P/B is high across MECO, showing only small fluctuations (1–2%; Figure 6). We therefore conclude that the decrease in CFAR probably was caused by decreased planktic foraminiferal (i.e., heterotroph) productivity rather than dissolution. We do not think it likely that a decrease in primary autotroph production caused the decline in CFAR and BFAR. Surface waters at Site 1263 would have been consistently nutrient poor due to its location within the subtropical gyre (Figure 1) and well-developed stratification (Figure 4) (see also *Winguth et al*. [2012] for the PETM). Further, FFAR remained constant, indicating that there was no significant change in calcareous nannoplankton productivity (i.e., autotroph primary productivity; Figure 6).

We also do not think it likely that a marked decrease in oxygen concentration in the mixed layer or deeper waters caused the decline in CFAR and BFAR. Crenarchaeol, the biomarker of ammonia oxidizing Archaea in the *phylum* Thaumarchaeota, increased across MECO (Figures 2 and 6), suggesting higher nitrification rates in the water column, for which oxygen is required. Planktic foraminiferal assemblages indicate normal oceanic conditions, and benthic foraminiferal assemblage composition indicates a well-oxygenated seafloor [*Boscolo Galazzo et al*., 2014].

We suggest that the differential temperature dependency of metabolic rates in photosynthesis and respiration could explain the accumulation rate patterns, as well as the increase in crenarchaeol abundance at Site 1263 across MECO. Biochemical reaction rates, metabolic rates, and nearly all other rates of biological activity increase exponentially with temperature [*Arrhenius*, 1889; *Brown et al*., 2004]. This relationship holds for all organisms, autotroph and heterotroph and ectothermic and endothermic, over the biologically relevant temperature range from 0° to 40°C [*Gillooly et al*., 2001; *Brown et al*., 2004]. Autotrophs, however, show a lesser increase in metabolic rates than heterotrophs for a specific increase in temperature [*O'Connor et al*., 2009].

Higher surface and deepwater temperatures during MECO would have increased metabolic rates, thus the demand for carbon and other nutrients to maintain basal metabolism, i.e., the energy required to stay alive [see also *Olivarez Lyle and Lyle*, 2006; *John et al*., 2013; *Ma et al*., 2014].

Constant FFAR across MECO may reflect the lesser response of photosynthetic rates to warming, coupled with population growth limitations imposed by nutrient availability [*O'Connor et al*., 2009]. The decrease in CFAR and BFAR during MECO may reflect the effect of the greater temperature-dependent increase of metabolic rates in heterotrophs [*O'Connor et al*., 2009]. Such differential metabolic scaling across trophic levels may have caused the decrease of heterotrophs including foraminifera, as primary productivity during MECO did not match their temperature-enhanced metabolic rates.

As an effect of temperature and consumer starvation, the remineralization of organic matter in the water column may have been higher, as has been argued for the PETM [*Ma et al*., 2014], increasing the concentration of ammonia available for oxidation. This may explain the increase of crenarchaeol across the MECO (Figures 2 and 6), as higher concentration of ammonia may have stimulated nitrification, which in open-ocean areas is mostly mediated by Archea in the *phylum* Thaumarchaeota [*Pearson and Ingalls*, 2013]. Increased recycling of organic matter in the water column would have at least reduced the amount of carbon available for sedimentation, further starving benthic foraminifera, as reflected in the decline in BFAR (Figure 6).

At Site 1263, as at other sites [*Luciani et al*., 2010; *Edgar et al*., 2013], the symbiont-bearing acarininids decreased in abundance across the MECO [*Luciani*, unpublished data, 2014]. This decrease has been previously attributed to loss of symbionts (bleaching) [*Edgar et al*., 2013]. Causes of bleaching are poorly known, and potential stress factors include high temperatures, high ultraviolet radiation, hypersalinity, starvation, and acidification [e.g., *Douglas*, 2003, and references therein]. We argue that starvation due to differential change in metabolic rates of the hosts (*Acarinina*) and their photosynthetic symbionts could have contributed to the decline of these muricate planktic foraminifera during MECO.

The MECO progressive warming may have thus directly affected the pelagic ecosystem structure at this subtropical gyre location, thus altering pelagic food webs and the recycling of organic carbon. This would have in turn affected the transfer of carbon to the ocean interior through the biological pump, with repercussions for the benthic fauna and the global carbon cycle.

Foraminiferal productivity only partially recovered during the cooling after the MECO (Figure 6), which could indicate that a longer time (>800 kyr) was necessary for recovery or that conditions did not return to those before MECO, resulting in overall lower productivity.

5.3. Carbon Isotope Records: Interpreting Global Carbon Cycling Over MECO

The carbon isotope signal of calcite tests is less affected by diagenesis and burial than the oxygen isotope signal [e.g., *Schrag et al*., 1995; *Pearson et al*., 2001; *Sexton et al*., 2006]. Although the oxygen isotope signal in *Acarinina* may be severely compromised, in most samples, its tests have higher $\delta^{13}C$ values than deeper calcifying *Globigerinatheka* (Figure 4), consistent with preferential uptake of ^{12}C during photosynthesis coupled with the biological pump [e.g., *Ridgwell*, 2011; *Sexton et al*., 2006]. Bulk $\delta^{13}C$ values reflect thermocline depths, with benthic values ~1.5‰ lower (Figures 4 and 5).

The primary features of the MECO carbon isotope records [*Bohaty et al*., 2009] include (1) a progressive, long-term increase in benthic and bulk $\delta^{13}C$ paralleling gradual warming; (2) a brief negative CIE coincident with the MECO peak; and (3) an interval of peak positive values in both benthic and bulk records between 39.9 and 39.2 Ma, shortly after the warmer phase. Unlike the PETM and other transient warming events, a significant negative CIE is not associated with the onset of warming [*Bohaty and Zachos*, 2003; *Bohaty et al*., 2009; *Sluijs et al*., 2013].

At Site 1263, benthic $\delta^{13}C$ values began to increase at ~40.7 Ma, peaking between 39.9 to 39.2 Ma (Figures 4 and 5), consistent with Southern Ocean benthic records (Figure 5) [*Bohaty et al*., 2009]. However, our benthic and planktic $\delta^{13}C$ records lack a negative CIE coincident with the MECO peak (−0.2‰) (Figures 4 and 5). Our bulk $\delta^{13}C$ values also lack a pronounced negative CIE (<−0.2‰) but become more positive after maximum warming (Figures 4 and 5). To explain the timing and pattern of warming and $\delta^{13}C$ values, *Bohaty et al*. [2009] hypothesized the enhanced degassing of relatively ^{13}C-enriched CO_2 from magmatic sources (i.e., volcanism) or metamorphic decarbonation in orogenic belts as the cause of the event. Indeed, an early stage of Ethiopian flood basalt activity might have occurred between 45 and 35 Ma [*George et al*., 1998], and the "Mid-Tertiary Ignimbrite Flare-Up" in Mexico started around 40–38 Ma [*Aguirre-Diaz and Labarthe-Hernandez*, 2003].

Positive feedback could have promoted further increases in CO_2 and temperatures over the ~500 kyr long MECO, including a decrease in the oceanic burial flux of organic and inorganic carbon (as described above) and a subsequent increase in the dissolved inorganic carbon (DIC) reservoir relative to the net weathering flux. Such a DIC increase would have lowered ocean pH and shoaled the CCD [*Lyle et al*., 2005; *Olivarez Lyle and Lyle*, 2006], consistent with CCD reconstructions [*Lyle et al*., 2005; *Pälike et al*., 2012] and in agreement with equatorial Pacific micropaleontological records across the MECO [*Toffanin et al*., 2013; *Takata et al*., 2013]. Calcium carbonate mass accumulation rates generally declined at sites deeper than 3 km in the equatorial Pacific, Indian Ocean, and SE Atlantic [*Bohaty et al*., 2009], which could reflect a widespread decrease in inorganic carbon burial during MECO. A gradual reduction in organic carbon flux due to enhanced heterotroph metabolic activities would have contributed to the progressive increase in $\delta^{13}C$ values in benthic foraminiferal records (Figure 5) [e.g., *Shackleton*, 1977].

A negative CIE is not clearly expressed in every record (Figure 1), and observed CIEs vary in magnitude (see Figure 4 in *Spofforth et al*. [2010]). Negative CIEs (~0.5‰) are present at high-southern latitude sections close to continental margins and in marginal Tethyan basins, including Sites 738, 748 (Figure 5; Southern Ocean, Kerguelen Plateau), and the Tethyan Alano section [*Bohaty et al*., 2009; *Edgar et al*., 2010; *Spofforth et al*., 2010]. Site 1051 (Blake Nose) has a small, negative CIE, and its exact timing is questionable (Figure 5) [*Bohaty et al*., 2009; *Edgar et al*., 2010]. Site 702 (Southern Ocean) has a small, negative CIE. The bulk $\delta^{13}C$ record at Site 689 (Weddell Sea, Southern Ocean) shows a slight negative $\delta^{13}C$ change [*Bohaty et al*., 2009], comparable with that at Site 1263 [*Bohaty et al*., 2009 this study]. At Site 523 (South Atlantic, Walvis Ridge), a CIE seems to be present, but a pulse of strong dissolution interrupted sedimentation in the critical

interval [*Bohaty et al*., 2009]. At the Contessa Highway and Monte Cagnero sections (central-western Tethys), the very noisy $\delta^{13}C$ signals [*Jovane et al*., 2007; *Savian et al*., 2013] make evaluation difficult, particularly at Contessa, but the Monte Cagnero record appears to lack a CIE. Thus, the degree and nature of the global carbon cycle disturbance during peak MECO as reflected in the available $\delta^{13}C$ records appear complex [*Sluijs et al*., 2013], and regional carbon cycle influences were likely important.

The apparent heterogeneity of the CIEs at MECO peak warming could be due to incomplete records of this short (~50 kyr) event at sites where sedimentation rates are low. However, even where the peak MECO CIE is present, it is considerably less pronounced (~0.5‰) than the CIEs during the early Eocene hyperthermals [e.g., *Lourens et al*., 2005; *Stap et al*., 2010; *McInerney and Wing*, 2011], though perhaps similar to the poorly characterized "hyperthermal events" of the early middle Eocene [*Sexton et al*., 2011]. In contrast, in duration, the CIE at peak MECO warming is comparable to post-PETM hyperthermals ETM2 and ETM3 [*Stap et al*., 2009; *Zachos et al*., 2010]. Threshold warming could have enhanced organic matter recycling, resulting in a brief pulse of isotopically depleted carbon from the ocean, as proposed for other small Eocene hyperthermals [*Sexton et al*., 2011] and consistent with the low BFAR and CFAR values at Site 1263.

An intriguing feature of the MECO is its abrupt termination. Enhanced silicate weathering may have led to an initial ~4°C temperature drop (Figures 2 and 4) when CO_2 degassing stopped, and cooling could have allowed recovery of the organic carbon burial flux, accelerating the sequestration of the excess of carbon [*Bowen and Zachos*, 2010]. The active hydrological cycle during peak warmth would have increased nutrient flux from land, further enhancing carbon burial flux in marginal ocean basins such as western Tethys. In marginal continental basins, eutrophication and deposition of organic-rich sediments are commonly associated with MECO warming and the period directly afterward [*Beniamovski et al*., 2003; *Spofforth et al*., 2010; *Boscolo Galazzo et al*., 2013]. An increase in organic carbon burial after the MECO might have been an efficient negative feedback to lower CO_2 levels, deepening the CCD [*Bohaty et al*., 2009; *Spofforth et al*., 2010] and leading to the abrupt increase in carbonate $\delta^{13}C$ values above the MECO peak warming interval (Figure 5) [*Jovane et al*., 2007; *Bohaty et al*., 2009; *Spofforth et al*., 2010; *Edgar et al*., 2010; *Savian et al*., 2013]. In addition, ending the enhanced organic matter remineralization in the open ocean as deduced for Site 1263 might has increased organic carbon storage in ocean sediments.

6. Summary and Conclusion

1. We present one of the first multiproxy investigations of the MECO in an open-ocean setting, providing new insight in this large climatic perturbation and its effects on ecosystems. The surface to bottom water temperature records at Site 1263 (Walvis Ridge, SE Atlantic Ocean) indicates a uniform warming of ~4°C throughout the water column, equivalent to warming at middle and high southern latitudes. Additional surface to bottom records across the MECO is needed in order to decipher the apparent leads and lags in our temperature records and determine whether they are at least in part a primary environmental signal.
2. Our biotic records suggest that during the MECO, the differential temperature-dependent increase of metabolic rates in autotrophs and heterotrophs altered the pelagic ecosystem with repercussions on the food web structure. Lack of nutrients in the surface waters at Site 1263 probably limited a temperature-induced increase in primary productivity, leading to heterotroph starvation, as seen in the significant decrease in planktonic foraminiferal accumulation rates, while autotroph nannoplankton accumulation rates remained stable. Higher metabolic rates would have also increased water column remineralization of organic matter, as indicated by an increase in the abundance of the chemoautotrophic ammonia-oxidizing Thaumarchaeota [*Pearson and Ingalls*, 2013] and reduced transport of organic carbon to the seafloor, as seen in decreased benthic foraminiferal accumulation rates. The effects of MECO on the primary productivity were not globally uniform, depending upon nutrient supply to meet enhanced metabolic rates of primary producers.
3. The $\delta^{13}C$ records are coherent with previously published records [*Bohaty et al*., 2009], but at Site 1263, the brief negative CIE during the MECO is not clearly present, with only slight negative variations in the benthic and bulk records. In general, the CIE during peak warming is much less pronounced and less consistently expressed than those of early Eocene hyperthermals [*Bohaty et al*., 2009; *Spofforth et al*., 2010]. This could be due to the short duration of the CIE and a lack of high-resolution records from expanded sections; our study could have inadequate time resolution in the critical interval. Alternately, the small amplitude of the CIE and its regional variability may reflect regional differences in carbon cycling superimposed on a global signal.

Acknowledgments
Data supporting this paper are available as in Table S1 in the supporting information. The samples were provided by the Ocean Drilling Program, and we thank the Bremen Core Repository for promptly handling our sample request. F.B.G.'s stay at Yale was funded by the Padova University financial support (Progetto di Ateneo GIUSPRAT10 CPDA108242/10 assigned to L.G. and ex 60% funding by Eliana Fornaciari) and a grant by the Geological Society of America to E.T., who also thanks the Leverhulme Foundation and recognizes funding through NSF grant OCE-0903014. F.B.G. thanks Peter Douglas, Srinath Krishnan, Guangsheng Zhuang, and Yi Ge Zhang for the laboratory assistance. The manuscript benefited from constructive reviews by three anonymous reviewers.

References

Aguirre-Diaz, G. J., and G. Labarthe-Hernandez (2003), Fissure ignimbrites: Fissure-source origin for voluminous ignimbrites of the Sierra Madre Occidental and its relationship with Basin and Range faulting, *Geology*, *31*, 773–776, doi:10.1130/G19665.1.

Arndt, S., B. B. Jørgensen, D. E. LaRowe, J. J. Middelburg, R. D. Pancost, and P. Regnier (2013), Quantifying the degradation of organic matter in marine sediments: A review and synthesis, *Earth Sci. Rev.*, *123*, 53–86, doi:10.1016/j.earscirev.2013.02.008.

Arrhenius, S. (1889), Über die Reaktionsgeschwindigkeit bei der Inversion von Rohrzucker in Säuren, *Z. Phys. Chem.*, *4*, 226–248.

Beniamovski, V. N., A. S. Alekseev, M. N. Ovechkina, and H. Oberhänsli (2003), Middle to Upper Eocene disoxic–anoxic Kuma Formation (northeast Peri-Tethys): Biostratigraphy and paleoenviroments, in *Causes and Consequences of Globally Warm Climates in the Early Paleogene*, edited by S. L. Wing et al., *Geol. Soc. Am. Spec. Pap.*, *369*, 95–112.

Berger, W. H., and L. Diester-Haass (1988), Paleoproductivity: The benthic/planktonic ratio in foraminifera as a productivity index, *Mar. Geol.*, *81*, 15–25, doi:10.1016/00253227(88)90014-X.

Bijl, P. K., A. J. P. Houben, S. Schouten, S. M. Bohaty, A. Sluijs, G. J. Reichart, J. S. Sinninghe Damsté, and H. Brinkhuis (2010), Transient middle Eocene atmospheric CO_2 and temperature variations, *Science*, *330*, 819–821, doi:10.1126/science.1193654.

Birch, H., H. K. Coxall, P. N. Pearson, D. Kroon, and M. O'Regan (2013), Planktonic foraminifera stable isotopes and water column structure: Disentangling ecological signals, *Mar. Micr.*, *101*, 127–145, doi:10.1016/j.marmicro.2013.02.002.

Boersma, A., I. Premoli Silva, and N. J. Shackleton (1987), Atlantic Eocene planktonic foraminiferal paleohydrographic indicators and stable isotope paleoceanography, *Paleoceanography*, *2*, 287–331, doi:10.1029/PA002i003p00287.

Bohaty, S. M., and J. C. Zachos (2003), A significant Southern Ocean warming event in the late middle Eocene, *Geology*, *31*, 1017–1020, doi:10.1130/G19800.1.

Bohaty, S. M., J. C. Zachos, F. Florindo, and M. L. Delaney (2009), Coupled greenhouse warming and deep-sea acidification in the Middle Eocene, *Paleoceanography*, *24*, PA2207, doi:10.1029/2008PA001676.

Borelli, C., B. S. Cramer, and M. E. Katz (2014), Bipolar Atlantic deepwater circulation in the middle late Eocene: Effects of Southern Ocean gateway openings, *Paleoceanography*, *29*, 308–327, doi:10.1002/2012PA002444.

Boscolo Galazzo, F., L. Giusberti, V. Luciani, and E. Thomas (2013), Paleoenvironmental changes during the Middle Eocene Climatic Optimum (MECO) and its aftermath: The benthic foraminiferal record from the Alano section (NE Italy), *Palaeogeogr. Palaeoclimatol. Palaeoecol.*, *378*, 22–35, doi:10.1016/j.palaeo.2013.03.018.

Boscolo Galazzo, F., E. Thomas, and L. Giusberti (2014), Benthic foraminiferal response to the Middle Eocene Climatic Optimum (MECO) in the South-Eastern Atlantic (ODP Site 1263), *Palaeogeogr. Palaeoclimatol. Palaeoecol.*, doi:10.1016/j.palaeo.2014.10.004.

Bowen, G. J., and J. C. Zachos (2010), Rapid carbon sequestration at the termination of the Palaeocene-Eocene Thermal Maximum, *Nat. Geosci.*, *3*, 866–869, doi:10.1038/ngeo1014.

Brown, J. H., J. F. Gillooly, A. P. Allen, V. M. Savage, and G. B. West (2004), Toward a metabolic theory of ecology, *Ecology*, *85*(7), 1771–1789.

Burgess, C. E., P. N. Pearson, C. H. Lear, H. E. G. Morgans, L. Handley, R. D. Pancost, and S. Schouten (2008), Middle Eocene climate cyclicity in the southern Pacific: Implications for global ice volume, *Geology*, *36*, 651–654, doi:10.1130/G24762A.1.

Cramer, B. S., J. D. W. D. V. Kent, and M.-P. Aubry (2003), Orbital climate forcing of $\delta^{13}C$ excursions in the late Paleocene–early Eocene (chrons C24n–C25n), *Paleoceanography*, *18*(4), 1097, doi:10.1029/2003PA000909.

Dawber, C. F., and A. K. Tripati (2011), Constraints on glaciation in the middle Eocene (46–37 Ma) from Ocean Drilling Program (ODP) Site 1209 in the tropical Pacific Ocean, *Paleoceanography*, *26*, PA2208, doi:10.1029/2010PA002037.

Diester-Haass, L. (1995), Middle Eocene to early Oligocene paleoceanography of the Antarctic Ocean (Maud Rise, ODP Leg 113, Site 689): Change from a low to a high productivity ocean, *Palaeogeogr. Palaeoclimatol. Palaeoecol.*, *113*, 311–334, doi:10.1016/0031-0182(95)00067-V.

Douglas, A. E. (2003), Coral bleaching – how and why?, *Mar. Pollut. Bull.*, *46*, 385–392, doi:10.1016/S0025-326X(03)00037-7.

Dunkley-Jones, T., D. J. Lunt, D. N. Schmidt, A. Ridgwell, A. Sluijs, P. J. Valdes, and M. Maslin (2013), Climate model and proxy data constraints on ocean warming across the Paleocene-Eocene Thermal maximum, *Earth Sci. Rev.*, *125*, 123–145, doi:10.1016/j.earscirev.2013.07.004.

Edgar, K. M., P. A. Wilson, P. F. Sexton, and Y. Suganuma (2007), No extreme bipolar glaciation during the main Eocene calcite compensation shift, *Nature*, *448*, 908–911, doi:10.1038/nature06053.

Edgar, K. M., P. A. Wilson, P. F. Sexton, S. J. Gibbs, A. P. Roberts, and R. D. Norris (2010), New biostratigraphic, magnetostratigraphic and isotopic insights into the Middle Eocene Climatic Optimum in low latitudes, *Palaeogeogr. Palaeoclimatol. Palaeoecol.*, *297*, 670–682, doi:10.1016/j.palaeo.2010.09.016.

Edgar, K. M., S. M. Bohaty, S. J. Gibbs, P. F. Sexton, R. D. Norris, and P. A. Wilson (2013), Symbiont 'bleaching' in planktic foraminifera during the Middle Eocene Climatic Optimum, *Geology*, *41*, 15–18, doi:10.1130/G33388.1.

Fietz, S., et al. (2012), Co-variation of crenarchaeol and branched GDGTs in globally-distributed marine and freshwater sedimentary archives, *Global Planet. Change*, *92*(93), 275–285, doi:10.1016/j.gloplacha.2012.05.020.

Fietz, S., F. G. Prahl, N. Moraleda, and A. Rosell-Melé (2013), Eolian transport of glycerol dialkyl glycerol tetraethers (GDGTs) off northwest Africa, *Org. Geochem.*, *64*, 112–118, doi:10.1016/j.orggeochem.2013.09.009.

Fornaciari, E., C. Agnini, R. Catanzariti, D. Rio, E. M. Bolla, and E. Valvasoni (2010), Mid-Latitude calcareous nannofossil biostratigraphy and biochronology across the middle to late Eocene transition, *Stratigraphy*, *7-4*, 229–264.

Galeotti, S., S. Krishnan, M. Pagani, L. Lanci, A. Gaudio, J. C. Zachos, S. Monechi, G. Morelli, and L. Lourens (2010), Orbital chronology of Early Eocene hyperthermals from the Contessa Road section, central Italy, *Earth Planet. Sci. Lett.*, *290*, 192–200, doi:10.1016/j.epsl.2009.12.021.

George, R., N. Rogers, and S. Kelley (1998), Earliest magmatism in Ethiopia: Evidence for two mantle plumes in one flood basalt province, *Geology*, *26*, 923–926, doi:10.1130/0091-7613.

Gillooly, J. F., E. L. Charnov, G. B. West, V. M. Savage, and J. H. Brown (2001), Effects of size and temperature on developmental time, *Nature*, *417*, 70–73.

Gooday, A. J. (2003), Benthic foraminifera (Protista) as tools in deep-water palaeoceanography: Environmental influences on faunal characteristics, *Adv. Mar. Biol.*, *46*, 1–90, doi:10.1016/S0065-2881(03)46002-1.

Hancock, H. J. L., and G. R. Dickens (2005), Carbonate dissolution episodes in Paleocene and Eocene sediment, Shatsky Rise, west central Pacific, in *Proc. Ocean Drill Program*, *Sci. Results*, vol. 198, pp. 1–24, Ocean Drilling Program, College Station, Tex., doi:10.2973/odp.proc.sr.198.116.2005.

Henson, S. A., R. Sanders, E. Madsen, P. J. Morris, F. Le Moigne, and G. D. Quartly (2011), A reduced estimate of the strength of the ocean's biological carbon pump, *Geophys. Res. Lett.*, *38*, L04606, doi:10.1029/2011GL046735.

Herguera, J. C., and W. Berger (1991), Paleoproductivity from benthonic foraminifera abundance: Glacial to postglacial change in the west-equatorial Pacific, *Geology*, *19*, 1173–1176, doi:10.1130/0091-7613.

Hoenisch, B., et al. (2012), The geological record of ocean acidification, *Science*, *335*, 1058–1063, doi:10.1126/science.1208277.

Holland, M. M., and C. M. Bitz (2003), Polar amplification of climate change in coupled models, *Clim. Dyn.*, *21*, 221–232, doi:10.1007/s00382-003-0332-6.

Hollis, C. J., et al. (2012), Early Paleogene temperature history of the Southwest Pacific Ocean: Reconciling proxies and models, *Earth Planet. Sci. Lett.*, *349–350*, 53–66, doi:10.1016/j.epsl.2012.06.024.

Hopmans, E. C., J. W. H. Weijers, E. Schefuss, L. Herfort, J. S. Sinninghe Damsté, and S. Schouten (2004), A novel proxy for terrestrial organic matter in sediments based on branched and isoprenoidal tetraether lipids, *Earth Planet. Sci. Lett.*, *224*, 107–116, doi:10.1016/j.epsl.2004.05.012.

Hu, J., P. A. Meyers, G. Chen, P. Peng, and Q. Yang (2012), Archaeal and bacterial glycerol dialkyl glycerol tetraethers in sediments from the Eastern Lau Spreading Center, South Pacific Ocean, *Org. Geochem.*, *43*, 162–167, doi:10.1016/j.orggeochem.2011.10.012.

Huber, M., and E. Thomas (2008), Paleoceanography: Greenhouse climates, in *Encyclopedia of Ocean Sciences*, edited by J. H. Steele, S. A. Thorpe, and K. K. Turekian, 2nd ed., pp. 4229–4239, Elsevier, New York, doi:10.1016/B978-012374473-9.00701.3.

Huber, M., L. C. Sloan, and C. Shellito (2003), Early Paleogene oceans and climate: A fully coupled modelling approach using NCAR's CCSM, in *Causes and Consequences of Globally Warm Climates in the Early Paleogene*, edited by S. L. Wing et al., *Geol. Soc. Am. Spec. Pap.*, *369*, 25–47.

Huguet, C., J. H. Kim, G. J. de Lange, J. S. Sinninghe Damsté, and S. Schouten (2009), Effects of long term oxic degradation on the U-37(K'), TEX_{86} and BIT organic proxies, *Org. Geochem.*, *40*, 1188–1194, doi:10.1016/j.orggeochem.2009.09.003.

Intergovernmental Panel on Climate Change (2001), Climate Change 2001: The scientific basis, in *Contribution of Working Group 1 to the Third Assessment Report of the Intergovernmental Panel on Climate Change*, edited by J. T. Houghton et al., pp. 881, Cambridge Univ. Press, Cambridge, U. K.

John, E. H., P. N. Pearson, H. K. Coxall, H. Birch, B. S. Wade, and G. L. Foster (2013), Warm ocean processes and carbon cycling in the Eocene, *Philos. Trans. R. Soc. A*, doi:10.1098/rsta.2013.0099.

Jorissen, F. J., C. Fontanier, and E. Thomas (2007), Paleoceanographical proxies based on deep-sea benthic foraminiferal assemblage characteristics, in *Developments in Marine Geology: Proxies in Late Cenozoic Paleoceanography*, vol. 1, edited by C. Hillaire-Marcel and A. de Vernal, pp. 264–325, Elsevier, Amsterdam.

Jovane, L., F. Florindo, R. Coccioni, J. Dinare's-Turell, A. Marsili, S. Monechi, A. P. Roberts, and M. Sprovieri (2007), The middle Eocene climatic optimum event in the Contessa Highway section, Umbrian Apennines, Italy, *Geol, Soc. Am. Bull.*, *119*, 413–427, doi:10.1130/B25917.1.

Katz, M. E., D. R. Katz, J. D. Wright, K. G. Miller, D. K. Pak, N. J. Shackleton, and E. Thomas (2003), Early Cenozoic benthic foraminiferal isotopes: Species reliability and interspecies correction factors, *Paleoceanography*, *18*(1), 1011, doi:10.1029/2002PA00079.

Kelly, D. C., T. J. Bralower, J. C. Zachos, I. Premoli-Silva, and E. Thomas (1996), Rapid diversification of planktonic foraminifera in the tropical Pacific (ODP Site 865) during the late Paleocene thermal maximum, *Geology*, *24*, 423–426, doi:10.1130/00917613(1996)024<0423:RDOPFI>2.3.CO;2.

Kim, J. H., J. van der Meer, S. Schouten, P. Helmke, V. Willmott, F. Sangiorgi, N. Koç, E. C. Hopmans, and S. Sinninghe Damsté (2010), New indices and calibrations derived from the distribution of crenarchaeal isoprenoid tetraether lipids: Implications for past sea surface temperature reconstructions, *Geochim. Cosmochim. Acta*, *74*, 4639–4654, doi:10.1016/j.gca.2010.05.027.

Klevenz, V., D. Vance, D. N. Schmidt, and K. Mezgera (2008), Neodymium isotopes in benthic foraminifera: Core-top systematics and a down-core record from the Neogene south Atlantic, *Earth Planet. Sci. Lett.*, *265*, 571–587, doi:10.1016/j.epsl.2007.10.053.

Kozdon, R., D. C. Kelly, N. T. Kita, J. H. Fournelle, and J. W. Valley (2011), Planktonic foraminiferal oxygen isotope analysis by ion microprobe technique suggests warm tropical sea surface temperatures during the Early Paleogene, *Paleoceanography*, *26*, PA3206, doi:10.1029/2010PA002056.

Lear, C. H., Y. Rosenthal, H. K. Coxall, and P. A. Wilson (2004), Late Eocene to early Miocene ice sheet dynamics and the global carbon cycle, *Paleoceanography*, *19*, PA4015, doi:10.1029/2004PA001039.

Lengger, S. K., M. Kraaij, R. Tjallingii, M. Baas, J.-B. Stuut, E. C. Hopmans, J. S. Sinninghe Damsté, and S. Schouten (2013), Differential degradation of intact polar and core glycerol dialkyl glycerol tetraether lipids upon post-depositional oxidation, *Org. Geochem.*, *65*, 83–93, doi:10.1016/j.orggeochem.2013.10.004.

Leon-Rodriguez, L., and G. R. Dickens (2010), Constraints on ocean acidification associated with rapid and massive carbon injections: The early Paleogene record at ocean drilling program site 1215, equatorial Pacific Ocean, *Palaeogeogr. Palaeoclimatol. Palaeoecol.*, *298*, 409–420, doi:10.1016/j.palaeo.2010.10.029.

Levitus, S., J. Antonov, and T. P. Boyer (1994), Interannual variability of temperature at a depth of 125 m in the North Atlantic Ocean, *Science*, *266*, 96–99.

Liu, Z., M. Pagani, D. Zinniker, R. DeConto, M. Huber, H. Brinkhuis, S. R. Shah, R. M. Leckie, and A. Pearson (2009), Global cooling during the Eocene-Oligocene climate transition, *Science*, *323*, 1187–1190, doi:10.1126/science.1166368.

Lourens, L. J., A. Sluijs, D. Kroon, J. C. Zachos, E. Thomas, U. Röhl, J. Bowles, and I. Raffi (2005), Astronomical pacing of late Palaeocene to early eocene global warming events, *Nature*, *435*, 1083–1087, doi:10.1038/nature03814.

Luciani, V., L. Giusberti, C. Agnini, E. Fornaciari, D. Rio, D. J. A. Spofforth, and H. Pälike (2010), Ecological and evolutionary response of Tethyan planktonic foraminifera to the middle Eocene climatic optimum (MECO) from the Alano section (NE Italy), *Palaeogeogr. Palaeoclimatol. Palaeoecol.*, *292*, 82–95, doi:10.1016/j.palaeo.2010.03.029.

Lunt, D., A. Ridgwell, A. Sluijs, J. Zachos, S. Hunter, and A. Haywood (2011), A model for orbital pacing of methane hydrate destabilization during the Palaeogene, *Nat. Geosci.*, *4*, 775–778, doi:10.1038/ngeo1266.

Lyle, M., A. Lyle Olivarez, J. Backman, and A. Tripati (2005), Biogenic sedimentation in the Eocene equatorial Pacific — The stuttering greenhouse and Eocene carbonate compensation depth, in *Proceedings of the Ocean Drilling Program*, *Sci. Results*, vol. 199, edited by P. A. Wilson, M. Lyle, and J. V. Firth, pp. 1–35, Ocean Drilling Program, College Station, Tex., doi:10.2973/odp.proc.sr.199.219.2005.

Lyle, M., J. Barron, T. J. Bralower, M. Huber, A. Olivarez Lyle, A. C. Ravelo, D. K. Rea, and P. A. Wilson (2008), Pacific Ocean and Cenozoic evolution of climate, *Rev. Geophys.*, *46*, RG2002, doi:10.1029/2005RG000190.

Ma, Z., E. Gray, E. Thomas, B. Murphy, J. C. Zachos, and A. Paytan (2014), Carbon sequestration during the Paleocene-Eocene Thermal maximum by an efficient biological pump, *Nat. Geosci.*, *7*, 382–388, doi:10.1038/NGEO2139.

McInerney, F. A., and S. L. Wing (2011), The Paleocene-Eocene thermal maximum: A perturbation of carbon cycle, climate, and biosphere with implications for the future, *Annu. Rev. Earth Planet. Sci.*, *39*, 489–516, doi:10.1146/annurev-earth-040610-133431.

Moebius, I., O. Friedrich, K. M. Edgar, H. D. Scher, and P. Sexton (2013), Bottom water changes in the subtropical North Atlantic and the Southern Ocean associated to the Middle Eocene Climatic Optimum, Abstract 1805987 presented at 2013 Fall Meeting, AGU, San Francisco, Calif., 9–13 Dec.

Moebius, I., O. Friedrich, and H. D. Scher (2014), Changes in Southern Ocean bottom water environments associated with the Middle Eocene Climatic Optimum (MECO), *Palaeogeogr. Palaeoclimatol. Palaeoecol.*, *405*, 16–27, doi:10.1016/j.palaeo.2014.04.004.

Moore, T. C., P. D. Rabinowitz, P. E. Borella, N. J. Shackleton, and A. Boersma (1984), History of the Walvis Ridge, in *Initial Reports of the Deep Sea Drilling Project*, vol. 74, edited by T. C. Moore Jr. and P. D. Rabinowitz, pp. 873–894, U.S. Government Printing Office, Wash.

O'Connor, M., M. F. Piehler, D. M. Leech, A. Anton, and J. F. Bruno (2009), Warming and resource availability shift food web structure and metabolism, *PLoS Biol.*, *7–8*, 1–6, doi:10.1371/journal.pbio.1000178.

Okada, H., and D. Bukry (1980), Supplementary modification and introduction of code numbers to the low-latitude coccolithbiostratigraphic zonation (Bukry, 1973;1975), *Mar. Micropaleontol.*, *5*, 321–325.

Olivarez Lyle, A., and M. W. Lyle (2006), Missing organic carbon in Eocene marine sediments: Is metabolism the biological feedback that maintains end-member climates?, *Paleoceanography*, *21*, PA2007, doi:10.1029/2005PA001230.

Pälike, H., R. D. Norris, J. O. Herrle, P. A. Wilson, H. K. Coxall, C. H. Lear, N. J. Shackleton, A. K. Tripati, and B. S. Wade (2006), The Heartbeat of the Oligocene Climate System, *Science*, *314*, 1894–1898.

Pälike, H., et al. (2012), A Cenozoic record of the equatorial Pacific carbonate compensation depth, *Nature*, *488*, 609–615, doi:10.1038/nature11360.

Pea, L. (2011), Eocene-Oligocene paleoceanography of the subantarctic South Atlantic: Calcareous Nannofossil reconstructions of temperature, nutrient, and dissolution history, PhD thesis, Dipartimento di Scienze della Terra, Università degli Studi di Parma, Parma, Italy.

Pearson, A., and A. E. Ingalls (2013), Assessing the Use of Archaeal Lipids as Marine Environmental Proxies, *Annu. Rev. Earth Planet. Sci.*, *41*, 359–384, doi:10.1146/annurev-earth-050212-123947.

Pearson, P. N. (2012), Oxygen isotopes in foraminifera: Overview and historical review, *Paleontol. Soc. Pap.*, *18*, 1–38.

Pearson, P. N., and M. R. Palmer (2000), Atmospheric carbon dioxide concentrations over the past 60 million years, *Nature*, *406*, 695–699, doi:10.1038/35021000.

Pearson, P. N., N. J. Shackleton, and M. A. Hall (1993), Stable isotope paleoecology of Middle Eocene planktonic foraminifera and multi-species isotope stratigraphy, DSDP Site 523, South Atlantic, *J. Foraminiferal Res.*, *23*, 123–140, doi:10.2113/gsjfr.23.2.123.

Pearson, P. N., P. W. Ditchfield, J. Singano, K. G. Harcourt-Brown, C. J. Nicholas, R. K. Olsson, N. J. Shackleton, and M. A. Hallk (2001), Warm tropical sea surface temperatures in the Late Cretaceous and Eocene epochs, *Nature*, *413*, 481–488, doi:10.1038/35097000.

Pearson, P. N., R. K. Olsson, C. Hemblen, B. T. Huber, and W. A. Berggren (2006), *Atlas of Eocene Planktonic Foraminifera*, *Cushman Spec. Publ.*, vol. 41, 513 pp., Cushman Foundation for Foraminiferal Research, Fredericksburg, Va.

Pearson, P. N., B. E. van Dongen, C. J. Nicholas, R. D. Pancost, S. Schouten, J. M. Singano, and B. S. Wade (2007), Stable warm tropical climate through the Eocene Epoch, *Geology*, *35*, 211–214, doi:10.1130/G23175A.1.

Penman, D. E., B. Hoenisch, R. E. Zeebe, E. Thomas, and J. C. Zachos (2014), Rapid and sustained surface ocean acidification during the Paleocene-Eocene Thermal maximum, *Paleoceanography*, *29*, 357–369, doi:10.1002/2014PA002621.

Peterse, F., J.-H. Kim, S. Schouten, K. D. Klitgaard, N. Koç, and J. S. Sinninghe Damsté (2009), Constraints on the application of the MBT/CBT palaeothermometer at high latitude environments (Svalbard, Norway), *Org. Geochem.*, *40*, 692–699, doi:10.1016/j.orggeochem.2009.03.004.

Premoli Silva, I., B. Wade, and P. N. Pearson (2006), Taxonomy, biostratigraphy, and phylogeny of *Globigerinatheka* and *Orbulinoides*, in *Atlas of Eocene Planktonic Foramifera*, *Cushman Found. Spec. Publ.*, vol. 41, edited by P. N. Pearson et al., pp. 169–212, Cushman Foundation for Foraminiferal Research, Fredericksburg, Va.

Ridgwell, A. (2011), Evolution of the ocean's "biological pump", *Proc. Natl. Acad. Sci. U.S.A.*, *108*, 16,485–16,486, doi:10.1073/pnas.1112236108.

Savian, J. F., Jovane, L., Trindade, R. I. F., Frontalini, F., Coccioni, R., Bohaty, S. M., Wilson, P. A., Florindo, F., and Roberts, A. (2013), Middle Eocene Climatic Optimum (MECO) in the Monte Cagnero Section, Central Italy, Latinmag Letters, 3, Special Issue, PC02, 1-8. Proceedings Montevideo, Uruguay.

Schouten, S., E. C. Hopmans, E. Schefuss, and J. S. Sinninghe Damsté (2002), Distributional variations in marine crenarchaeotal membrane lipids: A new tool for reconstructing ancient sea water temperatures?, *Earth Planet. Sci. Lett.*, *204*, 265–274, doi:10.1016/S0012-821X(02)00979-2.

Schouten, S., C. Huguet, E. C. Hopmans, M. V. M. Kienhuis, and J. S. Sinninghe Damste (2007), Analytical methodology for TEX_{86} paleothermometry by high-performance liquid chromatography/atmospheric pressure chemical ionization-mass spectrometry, *Anal. Chem.*, *79*, 2940–2944, doi:10.1021/ac062339v.

Schouten, S., et al. (2013), An interlaboratory study of TEX_{86} and BIT analysis of sediments, extracts, and standard mixtures, *Geochem. Geophys. Geosyst.*, *14*, 5263–5285, doi:10.1002/2013GC004904.

Schrag, D. P., D. J. Depaolo, and F. M. Richter (1995), Reconstructing past sea surface temperatures: Correcting for diagenesis of bulk marine carbonate, *Geochim. Cosmochim. Acta*, *59*, 2265–2278, doi:10.1016/0016-7037(95)00105-9.

Sexton, P. F., P. A. Wilson, and P. N. Pearson (2006), Microstructural and geochemical perspectives on planktic foraminiferal preservation: "Glassy" versus "Frosty", *Geochem. Geophys. Geosyst.*, *7*, Q12P19, doi:10.1029/2006GC001291.

Sexton, P. F., R. D. Norris, P. A. Wilson, H. Pälike, T. Westerhold, U. Röhl, C. T. Bolton, and S. Gibbs (2011), Eocene global warming events driven by ventilation of oceanic dissolved organic carbon, *Nature*, *471*, 349–352, doi:10.1038/nature09826.

Shackleton, N. J. (1974), Attainment of isotopic equilibrium between ocean water and the benthonic foraminifera genus *Uvigerina*: Isotopic changes in the ocean during the last glacial, in *Les Méthodes Quantitatives D'étude des Variations du Climat au Cours du Pléistocéne*, *Colloq. Int. C. N. R. S.*, vol. 219, pp. 203–209, Paris.

Shackleton, N. J. (1977), Carbon-13 in *Uvigerina*: Tropical rainforest history and the equatorial Pacific carbonate dissolution cycles, in *The Fate of Fossil Fuel CO_2 in the Oceans*, edited by N. R. Andersen and A. Malaho, pp. 401–447, Plenum Press, New York.

Shah, S. R., G. Mollenhauer, N. Ohkouchi, T. I. Eglinton, and A. Pearson (2008), Origins of archaeal tetraether lipids in sediments: Insights from radiocarbon analysis, *Geochim. Cosmochim. Acta*, *72*, 4577–4594, doi:10.1016/j.gca.2008.06.021.

Sluijs, A., G. J. Bowen, H. Brinkhuis, L. J. Lourens, and E. Thomas (2007), The Palaeocene-Eocene Thermal maximum super greenhouse: Biotic and geochemical signatures, age models and mechanisms of climate change, in *Deep-Time Perspectives on Climate Change: Marrying the Signal from Computer Models and Biological Proxies*, *Micropalaeontol. Soc. Spec. Publ.*, edited by M. Williams et al., pp. 323–349, The Geological Society, London.

Sluijs, A., R. E. Zeebe, P. K. Bijl, and S. M. Bohaty (2013), A middle Eocene carbon cycle conundrum, *Nat. Geosci.*, *6*(6), 429–434, doi:10.1038/NGEO1807.

Smith, R. W., T. S. Bianchi, and X. Li (2012), A re-evaluation of the use of branched GDGTs as terrestrial biomarkers: Implications for the BIT Index, *Geochim. Cosmochim. Acta*, *80*, 14–29, doi:10.1016/j.gca.2011.11.025.

Spero, H. J., and D. F. Williams (1988), Extracting Environmental information from planktonic foraminiferal delta-C-13 data, *Nature*, *335*, 717–719.

Spero, H. J., J. Bijma, D. W. Lea, and B. E. Bemis (1997), Effect of seawater carbonate concentration on foraminiferal carbon and oxygen isotopes, *Nature*, *390*, 497–500, doi:10.1038/37333.

Spofforth, D. J. A., C. Agnini, H. Pälike, D. Rio, E. Fornaciari, L. Giusberti, V. Luciani, L. Lanci, and G. Muttoni (2010), Organic carbon burial following the Middle Eocene Climatic Optimum (MECO) in the central-western Tethys, *Paleoceanography*, *25*, PA3210, doi:10.1029/2009PA00173.

Stap, L., L. J. Lourens, E. Thomas, A. Sluijs, S. Bohaty, and J. C. Zachos (2009), High-resolution deep-sea carbon and oxygen isotope records of Eocene Thermal Maximum 2 and H2, *Geology*, *38*, 208–210, doi:10.1130/G30777.1.

Stap, L., L. Lourens, A. van Dijk, S. Schouten, and E. Thomas (2010), Coherent pattern and timing of the carbon isotope excursion and warming during Eocene Thermal Maximum 2 as recorded in planktic and benthic foraminifera, *Geochem. Geophys. Geosyst.*, *11*, Q11011, doi:10.1029/2010GC003097.

Stoll, H. M. (2005), Limited range of interspecific vital effects in coccolith stable isotopic records during the Paleocene-Eocene thermal maximum, *Paleoceanography*, *20*, PA1007, doi:10.1029/2004PA001046.

Takata, H., R. Nomura, A. Tsujimoto, B. Khim, and I. Chung (2013), Abyssal benthic foraminifera in the eastern equatorial Pacific (IODP exp 320) during the Middle Eocene, *J. Paleontol.*, *87-6*, 1160–1185, doi:10.1666/12-107.

Thomas, D. J., and R. K. Via (2007), Neogene evolution of Atlantic thermohaline circulation: Perspective from Walvis Ridge, southeastern Atlantic Ocean, *Paleoceanography*, *22*, PA2212, doi:10.1029/2006PA001297.

Thomas, D. J., J. C. Zachos, T. J. Bralower, E. Thomas, and S. Bohaty (2002), Warming the Fuel for the Fire: Evidence for the thermal dissociation of methane hydrate during the Paleocene-Eocene thermal maximum, *Geology*, *30*, 1067–1070, doi:10.1130/0091-7613.

Thomas, E. (2003), Extinction and food at the seafloor: A high-resolution benthic foraminiferal record across the Initial Eocene Thermal Maximum, Southern Ocean Site 690, in *Colorado, Causes and Consequences of Globally Warm Climates in the Early Paleogene*, edited by S. L. Wing et al., *Geol. Soc. Am. Spec. Pap.*, *369*, 319–332.

Thomas, E., and N. J. Shackleton (1996), The Palaeocene-Eocene benthic foraminiferal extinction and stable isotope anomalies, in *Correlation of the Early Paleogene in Northwestern Europe*, edited by R. W. O. B. Knox, R. M. Corfield, and R. E. Dunay, *Geol. Soc. London Spec. Publ.*, *101*, 401–441.

Thomas, E., and J. C. Zachos (2000), Was the late Paleocene thermal maximum a unique event?, *GFF*, *122*, 169–170.

Thompson, J., G. T. Cook, R. Anderson, A. B. MacKenzie, D. D. Harkness, and I. N. McCave (1995), Radiocarbon age offsets in different-sized carbonate components of deep-sea sediments, *Radiocarbon*, *37*, 91–101.

Tierney, J. E., and M. P. Tingley (2014), A Bayesian, spatially-varying calibration model for the TEX_{86} proxy, *Geochim. Cosmochim. Acta*, *127*, 83–106, doi:10.1016/j.gca.2013.11.026.

Toffanin, F., C. Agnini, E. Fornaciari, D. Rio, L. Giusberti, V. Luciani, D. J. A. Spofforth, and H. Pälike (2011), Changes in calcareous nannofossil assemblages during the Middle Eocene Climatic Optimum: clues from the central-western Tethys (Alano section, NE Italy), *Mar. Micropaleontol.*, *81*, 22–31, doi:10.1016/j.marmicro.2011.07.002.

Toffanin, F., C. Agnini, D. Rio, G. Acton, and T. Westerhold (2013), Middle Eocene to early Oligocene calcareous nannofossil biostratigraphy at IODP Site U1333 (equatorial Pacific), *Micropaleontology*, *59–1*, 69–82.

Tripati, A., J. Backman, H. Elderfield, and P. Ferretti (2005), Eocene bipolar glaciations associated with global carbon cycle changes, *Nature*, *436*, 341–346, doi:10.1038/nature03874.

Van Morkhoven, F. P. C. M., W. A. Berggren, and A. S. Edwards (1986), Cenozoic Cosmopolitan deep-sea benthic foraminifera, *Bull. Cent. Rech. Explor. Prod. Elf-Aquitane*, *11*, 11–421.

Via, R. K., and D. J. Thomas (2006), Evolution of Atlantic thermohaline circulation–Early Oligocene onset of deep-water production in the North Atlantic, *Geology*, *34*, 441–444.

Villa, G., C. Fioroni, D. Persico, A. P. Roberts, and F. Florindo (2014), Middle Eocene to Late Oligocene glaciation/deglaciation and Southern Ocean productivity, *Paleoceanography*, *29*, 223–237, doi:10.1002/2013PA002518.

Wade, B. S. (2004), Planktonic foraminiferal biostratigraphy and mechanisms in the extinction of *Morozovella* in the late middle Eocene, *Mar. Micropaleontol.*, *51*, 23–38, doi:10.1016/j.marmicro.2003.09.001.

Wade, B. S., and D. Kroon (2002), Middle Eocene regional climate instability: Evidence from the western North Atlantic, *Geology*, *30*, 1011–1014, doi:10.1130/0091-7613.

Weijers, J. W. H., S. Schouten, O. C. Spaargaren, and J. S. Sinninghe Damsté (2006), Occurrence and distribution of tetraether membrane lipids in soils: Implications for the use of the TEX_{86} proxy and the BIT index, *Org. Geochem.*, *37*, 1680–1693, doi:10.1016/j.orggeochem.2006.07.018.

Westerhold, T., and U. Röhl (2013), Orbital pacing of Eocene climate during the Middle Eocene Climate Optimum and the chron C19r event: Missing link found in the tropical western Atlantic, *Geochem. Geophys. Geosyst.*, *14*, 4811–4825, doi:10.1002/ggge.20293.

Winguth, A., E. Thomas, and C. Winguth (2012), Global decline in ocean ventilation, oxygenation and productivity during the Paleocene-Eocene Thermal Maximum - Implications for the benthic extinction, *Geology*, *40*, 263–266, doi:10.1130/G32529.

Witkowski, J., S. M. Bohaty, K. McCartney, and D. M. Harwood (2012), Enhanced siliceous plankton productivity in response to middle Eocene warming at Southern Ocean ODP Sites 748 and 749, *Palaeogeogr. Palaeoclimatol. Palaeoecol.*, *326–328*, 78–94, doi:10.1016/j.palaeo.2012.02.006.

Witkowski, J., S. M. Bohaty, K. M. Edgar, and D. M. Harwood (2014), Rapid fluctuations in mid-latitude siliceous plankton production during the Middle Eocene Climatic Optimum (ODP Site 1051, western North Atlantic), *Mar. Micropaleontol.*, *106*, 110–129, doi:10.1016/j.marmicro.2014.01.001.

Zachos, J. C., L. D. Stott, and K. C. Lohmann (1994), Evolution of early Cenozoic marine temperatures, *Paleoceanography*, *9*, 353–387, doi:10.1029/93PA03266.

Zachos, J. C., et al. (2004), *Proceedings of the Ocean Drilling Program, Initial Rep.*, vol. 208, pp. 1–112, Texas A&M Univ., College Station, Tex.

Zachos, J. C., et al. (2005), Rapid acidification of the ocean during the Paleocene–Eocene Thermal Maximum, *Science*, *308*, 1611–1615, doi:10.1126/science.1109004.

Zachos, J. C., G. R. Dickens, and R. E. Zeebe (2008), An early Cenozoic perspective on greenhouse warming and carbon-cycle dynamics, *Nature*, *451*, 279–283, doi:10.1038/nature06588.

Zachos, J. C., H. K. McCarren, B. Murphy, U. Röhl, and T. Westerhold (2010), Tempo and scale of late Paleocene and early Eocene carbon isotope cycles: Implications for the origin of hyperthermals, *Earth Planet. Sci. Lett.*, *299*, 242–249, doi:10.1016/j.epsl.2010.09.004.

Zhang, Y., M. Pagani, Z. Liu, S. M. Bohaty, and R. DeConto (2013), A 40-million-year history of atmospheric CO_2, *Philos. Trans. R. Soc. A*, doi:10.1098/rsta.2013.0096.

Zhu, C., J. W. H. Weijers, T. Wagner, J.-M. Pan, J.-F. Chen, and R. D. Pancost (2011), Sources and distributions of tetraetherlipids in surface sediments across a large riverdominated continental margin, *Org. Geochem.*, *42*, 376–386, doi:10.1016/j.orggeochem.2011.02.002.